«ФИЗИКА ЭЛЕМЕНТАРНЫХ ЧАСТИЦ И АТОМНОГО ЯДРА»
1997, ТОМ 28, ВЫП.5

УДК 530.145

PHYSICS AT LHC

N.V.Krasnikov, V.A.Matveev

INR RAS, Moscow 117312

We review the physics to be investigated at LHC. We also describe the main parameters of CMS and ATLAS detectors.

Дается обзор физики, которая будет исследоваться на LHC. Описываются также основные параметры детекторов CMS и АТЛАС.

1. INTRODUCTION

The scientific programme at LHC (Large Hadron Collider) [1,2] which will be the biggest particle accelerator complex ever built in the world consists in many goals. Among them there are two supergoals:

a. Higgs boson discovery in standard electroweak Weinberg-Salam model.

b. Supersymmetry discovery.

LHC will accelerate two proton beams with the total energy $\sqrt{s} = 14$ TeV. At low luminosity stage (first two-three years of operation) the luminosity is planned to be $L_{low} = 10^{33}\text{cm}^{-2}s^{-1}$ with total luminosity $L_{tot} = 10^{4}\text{pb}^{-1}$ per year. At high luminosity stage the luminosity is planned to be $L_{high} = 10^{34}\text{cm}^{-2}s^{-1}$ with total luminosity $L_{tot} = 10^{5}\text{pb}^{-1}$ per year. The LHC will start to work in 2005 year. There are a lot of lines for research for LHC:

a. Higgs boson discovery in standard electroweak Weinberg-Salam model.

b. Supersymmetry discovery.

c. B-physics.

d. Heavy ion physics.

e. Top quark physics.

f. Standard physics (QCD, electroweak interactions).

g. The search for new physics beyond minimal supersymmetric model and Weinberg-Salam model.

There are planned to be two big detectors at LHC — CMS (compact muon solenoid) and ATLAS.

In this paper we describe the main parameters of CMS and ATLAS detectors and review the main physics to be investigated at LHC.*

*To be precise, we review the main physics to be investigated at CMS

2. DETECTORS

2.1. CMS Detector

Subdetectors. CMS detector consists of the following subdetectors:

1. Tracker barrel detector (TB).
2. Tracker forward detector (TF).
3. ECAL (electromagnetic calorimeter) barrel detector (EB).
4. ECAL forward (endcap) detector (EF).
5. Preshower in front of barrel ECAL (SB).
6. Preshower in front of forward ECAL (SF).
7. HCAL (hadronic calorimeter) barrel detector (HB).
8. HCAL forward (endcap) detector (HF).
9. Very forward calorimeter (VF).
10. Barrel muon station (MS).
11. Forward muon station (MF).

Basic Goals and Design Considerations. One of the most important tasks for LHC is the quest for the origin of the spontaneous symmetry-breaking mechanism in the electroweak sector of the standard model (SM). Namely, all the renormalizable models of electroweak interactions are based on the use of the gauge symmetry breaking. As a consequence of the electroweak symmetry breaking and the renormalizability of the theory there must be neutral scalar particle (Higgs boson) in the spectrum. The existing LEP1 bound on the Higgs boson mass in SM is $m_h \geq 64$ GeV., LEP2 with the full energy $\sqrt{s} = (190 - 195)$ GeV will be able to discover the Higgs boson in SM with a mass up to $m_h \leq (90 - 95)$ GeV. Theoretical bound based on tree-level unitarity gives upper bound $m_h \leq 1$ TeV for the Higgs boson mass. Lattice based estimates give similar bound $m_h \leq (700 - 800)$ GeV. In minimal supersymmetric extension of SM (MSSM) the lightest Higgs boson has to be relatively light $m_h \leq 120$ GeV. Other nonminimal supersymmetric models of electroweak interactions typically predict relatively light lightest Higgs boson $m_h \leq (160 - 180)$ GeV. So the discovery of the Higgs boson will be the check of the spontaneous symmetry breaking and the renormalizability of the theory and there are no doubts that it is the supergoal number 1 for LHC. The Higgs search is therefore used as a first benchmark for the detector optimization for both CMS and ATLAS. For the SM Higgs boson, the detector has to be sensitive to the following processes in order to cover the full mass range above the expected LEP2 discovery limit of $(90 - 95)$ GeV:

A. $h \to \gamma\gamma$ mass range 90 GeV$\leq m_h \leq$ 150 GeV.

B. $h \to b\bar{b}$ from $Wh, Zh, t\bar{t}h$ using $l^{\pm}(l^{\pm} = e^{\pm}$ or $\mu^{\pm})$- tag and b-tagging in the mass range 80 GeV$\leq m_h \leq$100 GeV.

C. $h \to ZZ^* \to 4l^{\pm}$ for mass range 130 GeV $\leq m_h \leq 2m_Z$.

D. $h \to ZZ \to 4l^{\pm}, 2l^{\pm}2\nu$ for the mass range $m_h \geq 2m_Z$.

E. $h \to WW, ZZ \to l^{\pm}\nu$ 2 jets, $2l^{\pm}$ 2 jets, using tagging of forward jets for m_h up to 1 TeV.

In minimal supersymmetric extension of the standard model (MSSM) there is a family of Higgs particles ($H^{\pm}, h, H$ and A). So in addition to the standard Higgs boson signatures the MSSM Higgs searches are based on the following processes:

F. $A \to \tau^+\tau^- \to e\mu$ plus $\nu's$, or $A \to \tau^+\tau^- \to l^{\pm}$ plus hadrons plus $\nu's$.

G. $H^{\pm} \to \tau^{\pm}\nu$ from $t\bar{t} \to H^{\pm}W^{\mp}b\bar{b}$ and $H^{\pm} \to 2$ jets, using a $l^{\pm}$- tag and b-tagging.

The observable cross sections for most of those processes are small, $(1 - 100)pb$ over a large part of the mass range. So it is necessary to work at high luminosity and to maximize the detectable rates above backgrounds by high-resolution measurements of electrons, muons and photons.

For the $H^{\pm}$ and A signatures in the case of the MSSM, high performance detector capabilities are required in addition for the measurements which are expected to be best achieved at initial luminosities with a low level of overlapping events, namely secondary vertex detection for τ-leptons and b-quarks, and high resolution calorimetry for jets and missing transverse energy E_T^{miss}.

The second supergoal of the LHC project is the supersymmetry discovery, i.e., the detection of superparticles. Here the main signature are the missing transverse energy events which are the consequence of the undetected lightest stable supersymmetric particles LSP predicted in supersymmetric models with R-parity conservation. Therefore it is necessary to set stringent requirements for the hermeticity and E_T^{miss} capability of the detector. Also the search for new physics different from supersymmetry (new gauge bosons W' and Z', new Higgs bosons with big Yukawa couplings, etc.) at LHC requires high resolution lepton measurements and charge identification even in the p_T range of a few TeV. Other possible signature of new physics (compositeness) can be provided by very high p_T jet measurements. An important task of LHC is the study of b- and t-physics. Even at low luminosities the LHC will be a high rate beauty- and top-quark factory. The main emphasis in B-physics is the precise measurement of CP-violation in the B_d^0-system and the determination of the Kobayashi-Maskawa angles. Besides investigations of $B\bar{B}$ mixing in the B_S^0-system, rare B-decays are also very important. Precise secondary vertex determination, full reconstruction of final states with relatively low-p_T particles, an example being $B_d^0 \to J/\Psi K_S^0$ followed by $J/\Psi \to l^+l^-$ and $K_S^0 \to \pi^+\pi^-$, and low-p_T lepton first-level triggering capability are all necessary. In addition to running as a proton-proton collider, LHC will be used to collide heavy ions at a centre of mass energy 5.5 TeV per nucleon pair. The formation of quark-gluon plasma in the heavy

ion collisions is predicted to be signalled by a strong suppression of Υ' and Υ'' production relative to Υ production when compared with pp-collisions. The CMS and ATLAS detectors will be used to detect low momentum muons produced in heavy ion collisions and reconstruct Υ, Υ', and Υ'' meson production. Therefore the basic design considerations for both ATLAS and CMS are the following:

1. Very good electromagnetic calorimetry for electron and photon identification and measurements,

2. Good hermetic jet and missing E_T-calorimetry,

3. Efficient tracking at high luminosity for lepton momentum measurements, for b-quark tagging, and for enhanced electron and photon identification, as well as tau and heavy-flavour vertexing and reconstruction capability of some B-decay final states at lower luminosity,

4. Stand-alone, precision, muon-momentum measurement up to the highest luminosity, and very low-p_T trigger capability at lower luminosity,

5. Large acceptance in η coverage.

Brief Description of CMS Subdetectors

Tracker. The design goal of the cental tracking system is to reconstruct isolated high-p_T tracks with an efficiency better than 95 percent, and high-p_T tracks within jets with an efficiency of better than 90 percent over the rapidity $|\eta| \leq 2.6$. The momentum resolution required for isolated charged leptons in the central rapidity region is $\frac{\delta p_T}{p_T} = 0.1 p_T$ (p_T in TeV). This will allow the measurement of the lepton charge up to $p_T = 2$ TeV. It is also very important for tracking system to perform efficient b- and τ-tagging. The tracker system consists of silicon pixels, silicon and gas microstrip detectors (MSGS) which provide precision momentum measurements and ensure efficient pattern of recognition even at the highest luminosity. A silicon pixel detectors consist of two barrel layers and three endcap layers and it is placed close to the beam pipe with the tasks of:

a. assisting in pattern recognition by providing two or three true space points per track over the full rapidity range in the main tracker,

b. improving the impact parameter resolution for b-tagging,

c. allowing 3-dimensional vertex reconstruction by providing a much improved Z-resolution in the barrel part.

The silicon microstrip detector is required to have a powerful vertex finding capability in the transverse plane over a large momentum range for b-tagging and heavy quark physics and must be able to distinguish different interaction vertices at high luminosity. The CMS silicon microstrip detector is subdivided into barrel and forward parts, meeting at $|\eta| = 1.8, \eta \equiv -\ln(\tan(\frac{\theta}{2}))$, provided at least 3 measuring points on each track for $|\eta| \leq 2.6$. The microstrip gas chambers provide a minimum of 7 hits for high-p_T tracks. The track finding

efficiency in the tracker is 98 per cent for $p_T \geq 5$ GeV. The charged particle momentum resolution depends on the η and p_T of charged particle and for $p_T = 100$ GeV and $|\eta| \leq 1.75$ it is around 2 per cent. Impact parameter resolution also depends on p_T and η and for 10 GeV$\leq p_T \leq 100$ GeV and $|\eta| \leq 1.3$ in transverse plane it is around 100 μm. The b-tagging efficiency from $\bar{t}t$-decays is supposed to be better than 30 per cent. A significant impact parameter can be used to tag τ-leptons. It could be useful in searches such as SUSY Higgs boson decays $A, H, h \to \tau\tau \to e + \mu + X(\text{or } l + hadrons)$. These leptons (hadrons) originate from secondary (τ) vertices while in the backgrounds from $\bar{t}t \to Wb + W\bar{b} \to e + \mu + X$ and $WW \to e + \mu + X$ they originate from the primary vertex. It is possible to have the efficiency for the signal ≈ 50 per cent while for the background channels it is ≈ 3 per cent.

ECAL. The barrel part of the electromagnetic calorimeter covers the rapidity intervals $|\eta| \leq 1.56$. The endcaps cover the intervals $1.65 \leq |\eta| \leq 2.61$. The gaps between the barrel and the endcaps are used to route the services of the tracker and preshower detectors. The barrel granularity is 432-fold in ϕ and 108×2-fold in η. A very good intrinsic energy resolution given by

$$\frac{\sigma}{E} = \frac{0.02}{\sqrt{E}} \oplus 0.005 \oplus \frac{0.2}{E} \tag{1}$$

is assumed to be for electrons and photons with a $PbWO_4$ crystal ECAL. The physics process that imposes the strictest performance requirements on the electromagnetic calorimeter is the intermediate Higgs mass decaying into two photons. The main goal here is to obtain very good di-photon mass resolution. The mass resolution has terms that depend on the resolution in energy (E_1, E_2) and the two-photon angular separation (θ) and it is given by

$$\frac{\sigma_M}{M} = \frac{1}{2}[\frac{\sigma_{E_1}}{E_1} \oplus \frac{\sigma_{E_2}}{E_2} \oplus \frac{\sigma_\theta}{\tan(\frac{\theta}{2})}], \tag{2}$$

where $\oplus$ denotes a quadratic sum, E is in GeV and θ is in radians. For the Higgs two-photon decay at LHC the angular term in the mass resolution can become important, so it is necessary to measure the direction of the photons using the information from the calorimeter alone. In the barrel region $|\eta| \leq 1.56$ angular resolution is supposed to be $\sigma_\theta \leq \frac{50\text{mrad}}{\sqrt{E}}$. Estimates give the following di-photon mass resolution for $h \to \gamma\gamma$ channel ($m_h = 100$ GeV):

$\delta m_{\gamma\gamma} = 475$ MeV (low luminosity $L = 10^{33}\text{cm}^{-2}s^{-1}$),
$\delta m_{\gamma\gamma} = 775$ MeV (high luminosity $L = 10^{34}\text{cm}^{-2}s^{-1}$).

HCAL. The hadron calorimeter surrounds the electromagnetic calorimeter and acts in conjunction with it to measure the energies and directions of particles and jets, and to provide hermetic coverage for measurement of the transverse

energy. The pseudorapidity range ($|\eta| \leq 3$) is covered by the barrel and endcap hadron calorimeters which sit inside the $4T$ field of CMS solenoid. In the central region around $\eta = 0$ a hadron shower 'tail catcher' is installed outside the solenoid coil to ensure adequate sampling depth. The active elements of the barrel and endcap hadron calorimeter consist of plastic scintillator tiles with wave length-shifting fibre readout. The pseudorapidity range ($3.0 \leq \eta \leq 5.0$) is covered by a separate very forward calorimeter. The hadron calorimeter must have good hermeticity, good transverse granularity, moderate energy resolution and sufficient depth for hadron shower containment. The physics programme requires good hadron resolution and segmentation to detect narrow states decaying into pairs of jets. The di-jet mass resolution includes contributions from physics effects such as fragmentation as well as detector effects such as angular and energy resolution. The energy resolution is assumed to be:

$$\frac{\Delta E}{E} = \frac{0.6}{\sqrt{E}} \oplus 0.03 \tag{3}$$

for $|\eta| \leq 1.5$ and segmentation $\Delta\eta \times \Delta\Phi = 0.1 \times 0.1$.

The di-jet mass resolution is approximately the following:

1. (10 -15) per cent for 50 GeV$\leq p_T \leq$ 60 GeV and $m_{ij} = m_Z$,
2. (5 - 10) per cent for 500 GeV$\leq p_T \leq$600 GeV and $m_{ij} = m_Z$.

The expected energy resolution for jets in the very forward calorimeter is parametrized by:

$$\frac{\sigma_{E_{jet}}}{E_{jet}} = \frac{1.28 \pm 0.1}{\sqrt{E_{jet}}} \oplus (0.02 \pm 0.01)\,. \tag{4}$$

The expected missing transverse energy resolution in the CMS detector with very forward $2.5 \leq \eta \leq 4.7$ coverage is

$$\frac{\sigma_t}{\sum E_t} = \frac{0.55}{\sqrt{\sum E_t}}\,, \tag{5}$$

(E_t in GeV). In the absence of the very forward calorimeter, the missing transverse energy resolution would be nearly three times worse.

Muon System. At the LHC the effective detection of muons from Higgs bosons, W, Z and $t\bar{t}$-decays requires coverage over a large rapidity interval. Muons from pp-collisions are expected to provide clean signatures for a wide range of new physics processes. Many of these processes are expected to be rare and will require the highest luminosity. The goal of the muon detector is to identify these muons and to provide a precision measurement of their momenta from a few GeV to a few TeV. The barrel detector covers the region $|\eta| \leq 1.3$. The endcap detector covers the region $1.3 \leq |\eta| \leq 2.4$. The muon detector should fulfil three basic tasks: muon identification, trigger and momentum measurement.

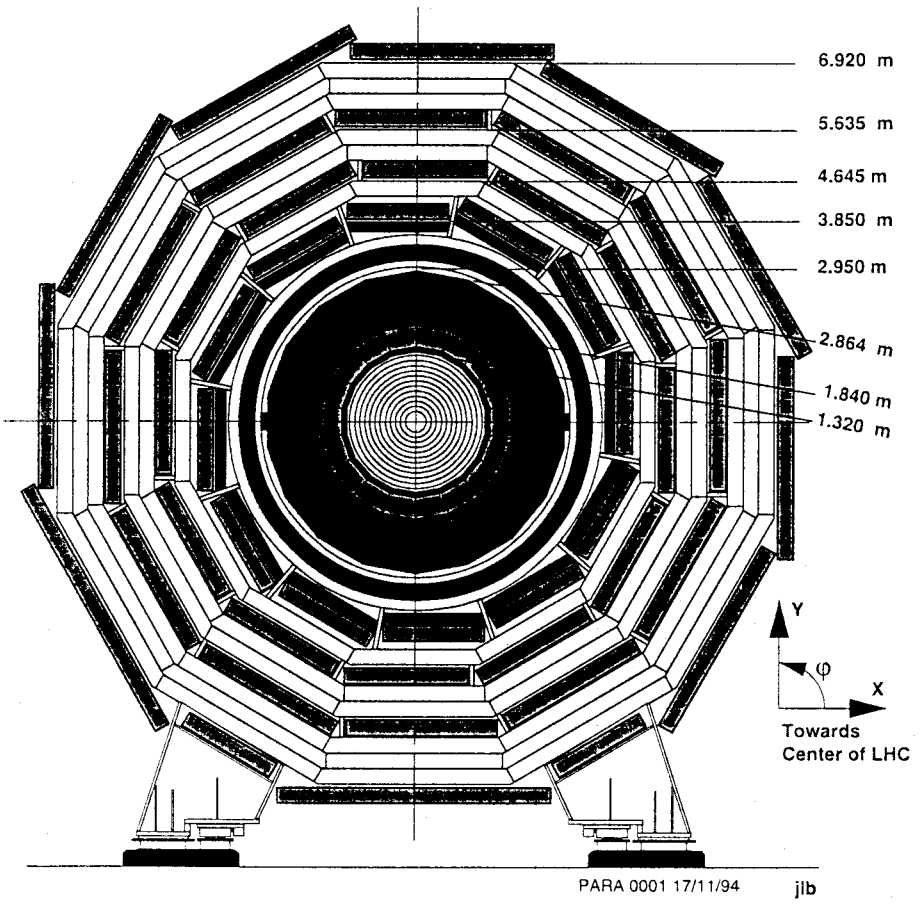

Fig. 2. Transverse view of the CMS detector

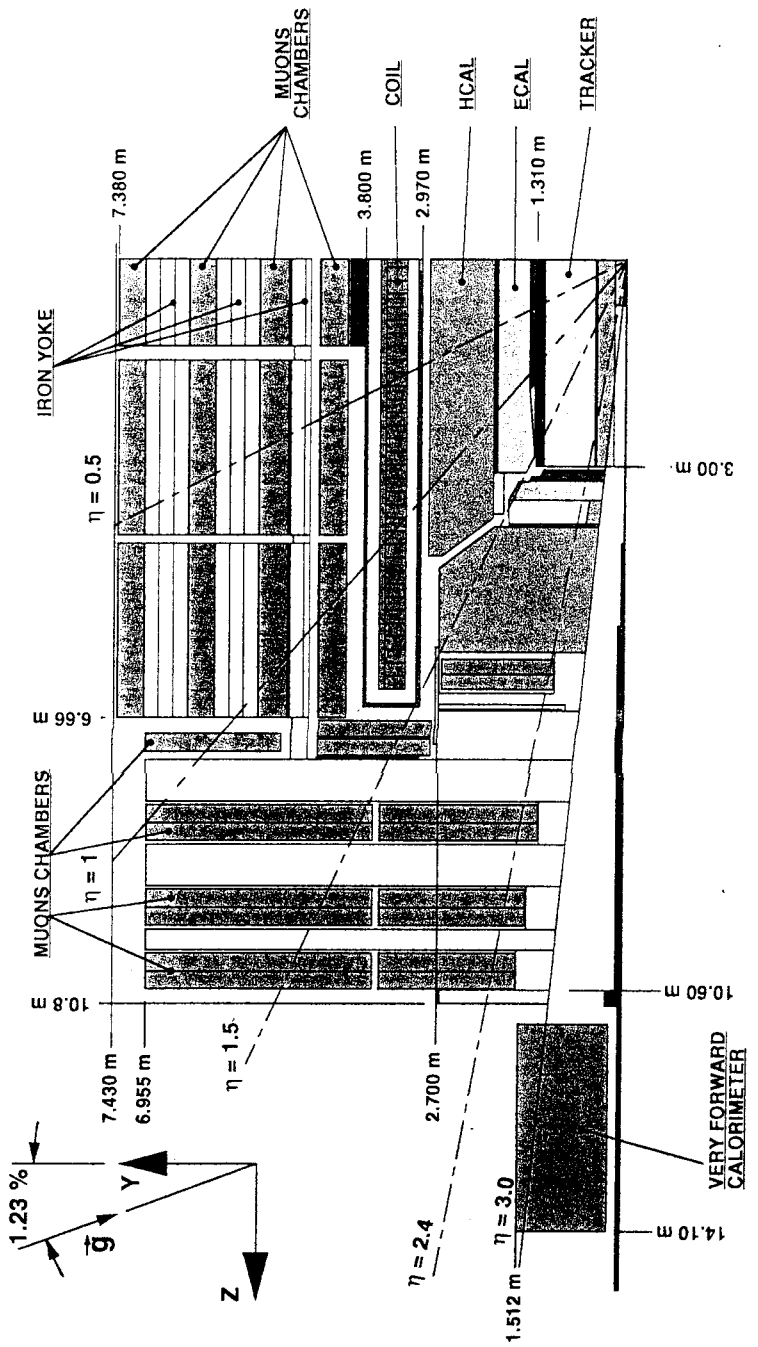

Fig. 3. Longitudinal view of the CMS detector

The muon detector is placed behind ECAL and the coil. It consists of four muon stations interleaved with the iron return yoke plates. The magnetic flux in the iron provides the possibility of an independent momentum measurement. The barrel muon detector is based on a system of 240 chambers of drift tubes arranged in four concentric stations. In the endcap regions, the muon detector comprises four muon stations. The muon detector has the following functionality and performance:

1. Geometric coverage: pseudorapidity coverage up to $|\eta| = 2.4$ with the minimum possible acceptance losses due to gaps and dead areas.

2. Transverse momentum resolution for the muon detector alone for $0 \leq |\eta| \leq 2$: $\frac{\Delta p_T}{p_T} = 0.06 - 0.1$ for $p_T = 10$ GeV, $0.07 - 0.2$ for $p_T = 100$ GeV and $0.15 - 0.35$ for $p_T = 1$ TeV.

3. Transverse momentum resolution after matching with central detector for $0 \leq |\eta| \leq 2$: $\frac{\Delta p_T}{p_T} = 0.005 - 0.01$ for $p_T = 10$ GeV, $0.015 - 0.05$ for $p_T = 100$ GeV and $0.05 - 0.2$ for $p_T = 1$ TeV.

4. Charge assignment: correct at 99 per cent confidence level up to $p_T = 7$ TeV for the full η coverage.

5. Muon trigger: precise muon chambers and fast dedicated detectors provide a trigger with p_T thresholds from a few GeV up to 100 GeV.

A schematic view of the CMS detector is shown in Figs.1, 2, and 3.

2.2. ATLAS Detector

The design of the ATLAS detector is similar to CMS detector. It also consists of inner detector (tracker), electromagnetic calorimeter, hadron calorimeter and muon spectrometer. Here we briefly describe the main parameters of the ATLAS subdetectors.

Inner Detector. The main parameters of the ATLAS inner detector are:

1. Tracking coverage over the pseudorapidity range $|\eta| \leq 2.5$.

2. Momentum resolution of $\frac{\Delta p_T}{p_T} \leq 0.3$ at $p_T = 500$ GeV for $|\eta| \leq 2$ and no worse than 50 per cent for $|\eta| = 2.5$.

3. Polar-angle resolution of ≤ 2 mrad.

4. Tracking efficiency of ≥ 95 per cent over the full coverage for isolated tracks with $p_T \geq 5$ GeV, with fake-track rates less than 1 per cent of signal rates.

5. Tagging of b-jets with an efficiency of ≥ 30 per cent at the highest luminosity, with a rejection ≥ 10 against non b-hadronic jets.

6. For initial lower-luminosity running the ability to reconstruct secondary vertices from b- and τ-decays and charged tracks from primary vertices and from secondary decay vertices of short-lived particles with ≥ 95 per cent efficiency for $p_T \geq 0.5$ GeV over the full coverage.

ECAL. The energy resolution is of $\frac{\Delta E}{E} = \frac{0.1}{\sqrt{E}} \oplus 0.007$ for $|\eta| \leq 2.5$. Diphoton mass resolution is estimated to be 1.4 GeV for Higgs boson mass $m_h = 100$ GeV

for $L = 10^{34}\mathrm{cm}^{-2}\mathrm{s}^{-1}$ (for CMS the diphoton mass resolution is 775 MeV).

HCAL. Jet energy resolution is of $\frac{\Delta E}{E} = \frac{0.5}{\sqrt{E}} \oplus 0.03$ for jets and a segmentation of $\Delta\eta \times \Delta\Phi = 0.1 \times 0.1$ for $|\eta| \leq 3$ and $\frac{\Delta E}{E} = \frac{1}{\sqrt{E}} \oplus 0.1$ and a segmentation of $\Delta\eta \times \Delta\Phi = 0.1 \times 0.1$ for very forward calorimeter $3 \leq |\eta| \leq 5$.

Muon Spectrometer. The muon momentum resolution is of $\frac{\Delta p_T}{p_T} = 0.02(p_T = 20$ GeV), $\frac{\Delta p_T}{p_T} = 0.02(p_T = 100$ GeV), $\frac{\Delta p_T}{p_T} = 0.08(p_T = 1$ TeV) for $|\eta| \leq 3$.

3. PHYSICS AT LHC

3.1. Parton Model

A high-energy proton beam may be regarded as an unseparated beam of quarks, antiquarks and gluons. For the hard-scattering phenomena that are the principal interest of LHC the cross section for the hadronic reaction

$$a + b \to c + anything \tag{6}$$

is given in parton model by the formula [3,4]

$$d\sigma(a + b \to c + X) = \sum_{partons:i,j} f_i^{(a)} f_j^{(b)} d\hat{\sigma}(i + j \to c + X'), \tag{7}$$

where $f_i^{(a)}$ is the probability of finding constituent i in hadron a and $\hat{\sigma}(i + j \to c + X')$ is the cross section for the elementary process leading to the desired final state. This picture of hadron collisions in many cases provides a reliable estimate of cross sections. Two ingredients are required to compute cross sections: the elementary cross sections and the parton distributions. It is straightforward to calculate the elementary cross sections, at least at low orders in perturbation theory. At given scale, the parton distributions can be measured in deep inelastic lepton-hadron scattering. The evolution of these distributions to larger momentum scales is described by perturbative QCD.

As has been mentioned before, the main idea of parton model is to regard a high energy proton as a collection of quasi-free partons which share its momentum. Thus we consider a proton with momentum P as being made of partons carrying longitudinal momenta $x_i P$, where the momentum fractions x_i satisfy

$$0 \leq x_i \leq 1 \tag{8}$$

and

$$\sum_{partons\, i} x_i = 1\,. \tag{9}$$

The cross section for the reaction (6) is given by

$$d\sigma(a+b\to c+X)=\sum_{ij} f_i^{(a)}(x_a)f_j^{(b)}(x_b)d\hat{\sigma}(i+j\to c+X')\,, \qquad (10)$$

where $f_i^{(a)}(x)$ is the number distribution of partons of species i. The summation runs over all contributing parton configurations. Let us denote the invariant mass of the $i-j$ system as

$$\sqrt{\hat{s}}=\sqrt{s\tau} \qquad (11)$$

and its longitudinal momentum in the hadron-hadron c.m. by

$$p=x\sqrt{s}/2\,. \qquad (12)$$

The kinematic variables $x_{a,b}$ of the elementary process are related to those of the hadronic process by

$$x_{a,b}=\frac{1}{2}[(x^2+4\tau)^{1/2}\pm x]\,. \qquad (13)$$

The parton momentum fractions satisfy the relations

$$x_a x_b=\tau\,, \qquad (14)$$

$$x_a-x_b=x\,. \qquad (15)$$

The elementary parton model as described here does not take into account QCD strong interaction effects. The most important modification of naive parton model is due to QCD corrections to the parton distributions. In leading logarithmic approximation [5] these corrections are process independent and can be incorporated by the replacement

$$f_i^{(a)}(x_a)\to f_i^{(a)}(x_a,Q^2)\,. \qquad (16)$$

There is some ambiguity in the choice of scale Q^2 for a particular process. It should be of the order of the subenergy $Q^2\approx\hat{s}$. The knowledge of the next to leading corrections allows one to fix the scale Q^2. Usually we shall neglect higher-order QCD corrections. Experience shows that in many cases an account of higher order corrections increases the value of cross sections by a factor of $1.5-2$ [5].

To calculate production cross sections for a hadron collider we have to know parton distributions as functions of the scaling variable x and Q^2. For the study of a process with characteristic mass M, the parton distributions must be known for $Q^2\approx M^2$ and $x\geq M^2/s$. The typical momentum fraction contributing to such a process is $x\approx M/\sqrt{s}$. We shall be interested in masses $M\geq O(100)$ GeV, so for LHC $x\geq O(10^{-2})$ and $Q^2\geq O(10^4)\ GeV^2$. Although the distributions have not been measured at such values of Q^2, it is possible to obtain them using the Altarelli-Parisi equation and the parton distributions at some scale Q_0^2. It is convenient to parametrize the distributions in a valence plus sea plus gluon form.

The proton contains:
up quarks: $u_v(x,Q^2)+u_s(x,Q^2)$,
down quarks: $d_v(x,Q^2)+d_s(x,Q^2)$,
up antiquarks $u_s(x,Q^2)$,
down antiquarks: $d_s(x,Q^2)$,
strange, charm, bottom and top quarks and antiquarks: $q_s(x,Q^2)$,
gluons: $G(x,Q^2)$.

The flavour quantum numbers of the proton are carried by the valence quarks. Those distributions must therefore satisfy the number sum rules

$$\int_0^1 dx\, u_v(x,Q^2) = 2\,, \tag{17}$$

$$\int_0^1 dx\, d_v(x,Q^2) = 1\,. \tag{18}$$

The parton distributions are also constrained by the momentum sum rule

$$\int_0^1 dx\, x[u_v + d_v + G + 2(u_s + d_s + s_s + c_s + b_s + t_s)] = 1\,. \tag{19}$$

For protons, many sets of parton distributions exist on the market. These are obtained by fits to experimental data, constrained so that the Q^2 dependence is in accordance with the standard QCD evolution equations. At present the most popular set of parton distributions is CTEQ2L [6]. Also available in PYTHIA program [7] are EHLQ, DO, CTEQ2M, CTEQ2MS, CTEQ2MF, CTEQ2ML and CTEQ2D sets of parton distributions. The Altarelli-Parisi equation for nonsinglet distributions reads

$$\frac{dp(x,Q^2)}{d\ln Q^2} = \frac{2\alpha_s(Q^2)}{3\pi}\int_x^1 dz[\frac{(1+z^2)p(y,Q^2)-2p(x,Q^2)}{1-z}] + \frac{\alpha_s(Q^2)}{\pi}[1+\frac{4\ln(1-x)}{3}]p(x,Q^2)\,, \tag{20}$$

where

$$p(x,Q^2) = xu_v(x,Q^2)\ or\ xd_v(x,Q^2) \tag{21}$$

and $y = x/z$. The evolution of the gluon momentum distribution

$$g(x,Q^2) = xG(x,Q^2) \tag{22}$$

is given by

$$\frac{dg(x,Q^2)}{d\ln Q^2} = \frac{\alpha_s(Q^2)}{\pi}\int_x^1 dz[\frac{3[zg(y,Q^2)-g(x,Q^2)]}{1-z} +$$

$$\frac{3(1-z)(1+z^2)g(y,Q^2)}{z}+\frac{2}{3}\frac{1+(1-z)^2}{z}\times$$
$$\sum_{flavors:q} y[q_v(y,Q^2)+2q_s(y,Q^2)]+\frac{\alpha_s(Q^2)}{\pi}[\frac{11}{4}$$
$$-\frac{N_f}{6}+3\ln(1-x)]g(x,Q^2)\,, \tag{23}$$

where N_f is the number of flavours participating in the evolution at Q^2. The evolution of the momentum distributions of the light sea-quarks

$$l(x,Q^2)=xu_s(x,Q^2)\ or\ xd_s(x,Q^2)\ or\ xs_s(x,Q^2) \tag{24}$$

is described by

$$\frac{dl(x,Q^2)}{d\ln Q^2}=\frac{2\alpha_s(Q^2)}{3\pi}\int_x^1 dz[\frac{(1+z^2)l(y,Q^2)-2l(x,Q^2)}{1-z}+ \tag{25}$$
$$\frac{3}{8}[z^2+(1-z)^2]g(y,Q^2)]+\frac{\alpha_s(Q^2)}{\pi}[1+\frac{4}{3}\ln(1-x)]l(x,Q^2)\,.$$

For the evolution of the momentum distributions of heavy sea quarks

$$h(x,Q^2)=xc_s(x,Q^2)\ or\ xb_s(x,Q^2)\ or\ xt_s(x,Q^2) \tag{26}$$

the evolution equation reads [8]

$$\frac{dh(x,Q^2)}{d\ln Q^2}=\frac{2\alpha_s(Q^2)}{3\pi}\int_x^1 dz[\frac{(1+z^2)h(y,Q^2)-2h(x,Q^2)}{1-z}+ \tag{27}$$
$$\frac{3}{4\beta}[\frac{1}{2}-z(1-z)+\frac{M_q^2}{Q^2}\frac{(3-4z)z}{1-z}-\frac{16M_q^4z^2}{Q^4}]g(y,Q^2)-$$
$$\frac{3M_q^2}{2Q^2}[z(1-3z)+\frac{4M_q^2z^2}{Q^2}]$$
$$\ln(\frac{1+\beta}{1-\beta})g(y,Q^2)]\theta(\beta^2)+\frac{\alpha_s(Q^2)}{\pi}[1+\ln(1-x)]h(x,Q^2)\,,$$

where M_q is the heavy quark mass and

$$\beta=[1-4M_q^2/Q^2(1-z)]^{1/2}\,. \tag{28}$$

The formula for the running effective strong coupling constant for massless quarks in the leading log approximation has the form

$$\alpha_s(Q^2)=\frac{12\pi}{(33-12N_f)\ln(Q^2/\Lambda^2)}\,. \tag{29}$$

We shall use the formula (29) for $N_f = 4$. For the case of massive quarks the generalization of the formula (29) takes the form

$$1/\alpha_s(Q^2) = \frac{25}{12\pi}\ln(Q^2/\Lambda^2) - \frac{1}{6\pi}\sum_{i=b,t,\ldots}\theta(Q^2 - 16M_i^2)\ln(Q^2/16M_i^2)\,. \quad (30)$$

The parton distributions are necessary to calculate differential and total cross sections. It appears that the cross sections depend on some particular combination of structure functions, parton-parton luminosities. Namely, the differential cross section for the reaction

$$a + b \to \alpha + anything \quad (31)$$

is given by

$$\frac{d\sigma}{d\tau}(a + b \to \alpha + X) = \sum_{ij}\frac{dL_{ij}}{d\tau}\hat{\sigma}(ij \to \alpha)\,, \quad (32)$$

where $\hat{\sigma}(ij \to \alpha)$ is the cross section for the corresponding elementary process, $\tau = \hat{s}/s$ and

$$\frac{dL_{ij}}{d\tau} = \frac{1}{1+\delta_{ij}}\int_\tau^1 dx[f_i^{(a)}(x)f_j^{(b)}(\tau/x) + f_j^{(a)}(x)f_i^{(b)}(\tau/x)]/x\,. \quad (33)$$

Here $f_i^{(a)}(x)$ is the number distribution of partons of species i carrying momentum fraction x of hadron a. The hard-scattering processes that determine the study for interesting physics at LHC have a common asymptotic form prescribed by dimensional analysis

$$\sigma(\hat{s}) = c/\hat{s}\,. \quad (34)$$

For a strong-interaction process, such as jet pair production, c is typically of order $(\alpha_s/\pi)^2$. For a typical electroweak process such as lepton pair production, c is approximately $(\alpha/\pi)^2$. Resonance production cross sections are proportional to τ. Therefore the quantity $\frac{\tau}{\hat{s}}\frac{dL}{d\tau}$, which has dimension of the cross section, provides a useful measure of the reach of hadron collider at given energy and hadron-hadron luminosity.

3.2. Physics within SM

3.2.1. Top-Quark Physics

Even at low initial luminosities of $10^{32}\mathrm{cm}^{-2}\mathrm{s}^{-1}$ approximately 6000 $t\bar{t}$ pairs would be produced per day at $m_t = 170$ GeV, yielding about 100 reconstructed $t\bar{t} \to (l\nu b)(jjb)$ decays per day and about 10 clean isolated $e\mu$ pairs per day. The $t \to jjb$ decays provide an abundant event sample, which allows direct reconstruction of m_t, through the invariant mass of 3-jet system. The conclusion is that the ultimate accuracy of ± 2 GeV may be achieved for $m_t = 170$ GeV [2].

Multilepton events from top-quark decays can also be used to extract an accurate measurement of m_t. The most promising method is to use 2 leptons from the same top-quark decay. For an integrated luminosity of 10^4pb^{-1}, the expected statistical uncertainty on the measurement of m_t, using this method, is approximately ± 0.5 GeV for $m_t = 170$ GeV. The overall systematic uncertainty due to fragmentation effects will very likely to be less than ± 2 GeV. The conclusion is that the accuracy of better than ± 2 GeV may be achieved in this channel.

3.2.2. Higgs Boson in the Weinberg-Salam Model

The standard Weinberg-Salam model is the renormalizable model of strong and electroweak interactions. It has the gauge group $SU_c(3) \otimes SU(2)_L \otimes U(1)$ and the minimal Higgs structure consisting of one complex doublet of scalar particles. The spontaneous electroweak symmetry breaking $SU_c(3) \otimes SU_L(2) \otimes U(1) \to SU_c(3) \otimes U(1)$ due to nonzero vacuum expectation value of the Higgs doublet provides the simplest realization of the Higgs mechanism [9] which generates masses for $W^{\pm}$, Z gauge bosons and masses to quarks and leptons. In this approach, the Goldstone bosons are generated by dynamics of elementary scalar fields and precisely one neutral Higgs scalar (the Higgs boson) remains in the physical spectrum. The Lagrangian of Weinberg-Salam model consists of several pieces [10]:

$$L_{WS} = L_{YM} + L_{HYM} + L_{SH} + L_f + L_{Yuk} \,. \tag{35}$$

Here L_{YM} is the Yang-Mills Lagrangian without matter fields

$$L_{YM} = -\frac{1}{4} F^i_{\mu\nu}(W) F^{\mu\nu}_i(W) - \frac{1}{4} F^{\mu\nu}(W^0) F_{\mu\nu}(W^0) - \frac{1}{4} F^a_{\mu\nu}(G) F^{\mu\nu}_a(G) \,, \tag{36}$$

where $F^i_{\mu\nu}(W)$, $F^a_{\mu\nu}(G)$, $F_{\mu\nu}(W^0)$ are given by

$$F^i_{\mu\nu}(W) = \partial_\mu W^i_\nu - \partial_\nu W^i_\mu + g_2 \epsilon^{ijk} W^j_\mu W^k_\nu \,, \tag{37}$$

$$F_{\mu\nu}(W^0) = \partial_\mu W^0_\nu - \partial_\nu W^0_\mu \,, \tag{38}$$

$$F^a_{\mu\nu}(G) = \partial_\mu G^a_\nu - \partial_\nu G^a_\mu + g_s f^{abc} G^b_\mu G^c_\nu \,, \tag{39}$$

where W^i_μ, W^0_μ are the $SU_L(2) \otimes U(1)$ gauge fields, G^a_μ are the gluon fields and ϵ^{ijk}, f^{abc} are the structure constants of the $SU(2)$ and $SU(3)$ gauge groups. The Lagrangian L_{HYM} describes the Higgs doublet interaction with $SU_L(2) \otimes U(1)$ gauge fields

$$L_{HYM} = (D_{L\mu} H)^+ (D^\mu_L H) \,, \tag{40}$$

where covariant derivatives are given by

$$D_{L\mu} = \partial_\mu - i g_1 \frac{Y}{2} W^0_\mu - i g_2 \frac{\sigma^i}{2} W^i_\mu \,, \tag{41}$$

$$D_{R\mu} = \partial_\mu - ig_1 \frac{Y}{2} W_\mu^0 , \tag{42}$$

$$D_{L\mu}^q = \partial_\mu - ig_1 \frac{Y}{2} W_\mu^0 - ig_2 \frac{\sigma^i}{2} W_\mu^i - ig_s t^a G_\mu^a , \tag{43}$$

$$D_{R\mu}^q = \partial_\mu - ig_1 \frac{Y}{2} W_\mu^0 - ig_s t^a G_\mu^a . \tag{44}$$

Here g_1 is the $U(1)$ gauge coupling constant, Y is the hypercharge determined by the relation $Q = \frac{\sigma_3}{2} + \frac{Y}{2}$, σ^i are Pauli matrices, t^a are $SU(3)$ matrices in the fundamental representation, $H = \begin{pmatrix} H_1 \\ H_2 \end{pmatrix}$ is the Higgs $SU(2)$ doublet with $Y = 1$. The Lagrangian L_{SH} describing Higgs doublet self-interaction has the form

$$L_{SH} = -V_0(H) = M^2 H^+ H - \frac{\lambda}{2}(H^+ H)^2 , \tag{45}$$

where $H^+ H = \sum_i H_i^* H_i$ and λ is the Higgs self-coupling constant. Lagrangian L_f describes the interaction of fermions with gauge fields. Fermions constitute only doublets and singlets in $SU_L(2) \otimes U(1)$

$$R_1 = e_R,\ R_2 = \mu_R,\ R_3 = \tau_R , \tag{46}$$

$$L_1 = \begin{pmatrix} \nu \\ e \end{pmatrix}_L L_2 = \begin{pmatrix} \nu' \\ \mu \end{pmatrix}_L L_3 = \begin{pmatrix} \nu'' \\ \tau \end{pmatrix}_L , \tag{47}$$

$$R_{qIu} = (q_{Iu})_R,\ \ (q_{1u} = u,\ q_{2u} = c,\ q_{3u} = t) , \tag{48}$$

$$. R_{qid} = (q_{id})_R,\ \ (q_{1d} = d,\ q_{2d} = s,\ q_{3d} = b) , \tag{49}$$

$$L_{qI} = \begin{pmatrix} q_{Iu} \\ V_{Ii} q_{id} \end{pmatrix}_L , \tag{50}$$

where L and R denote left- and right-handed components of the spinors, respectively,

$$\psi_{R,L} = \frac{1 \pm \gamma_5}{2} \psi \tag{51}$$

and V_{il} is the Kobayashi-Maskawa matrix. The neutrinos are assumed to be left-handed and massless. The Lagrangian L_f has the form

$$L_f = \sum_{k=1}^{3} [i\bar{L}_k \hat{D}_L L_k + i\bar{R}_k \hat{D}_R R_k + i\bar{L}_{qk} \hat{D}_L^q L_{qk} + i\bar{R}_{qku} \hat{D}_R^q R_{qku} + i\bar{R}_{qkd} \hat{D}_R^q R_{qkd}] , \tag{52}$$

where $\hat{D}_L = \gamma^\mu D_{L\mu}$, $\hat{D}_R = \gamma^\mu D_{R\mu}$, $\hat{D}^q_L = \gamma^\mu D^q_{L\mu}$, $\hat{D}^q_R = \gamma^\mu D^q_{R\mu}$. The Lagrangian L_{Yuk} generates fermion mass terms. Supposing the neutrinos to be massless, the Yukawa interaction of the fermions with Higgs doublet has the form

$$L_{Yuk} = -\sum_{k=1}^{3}[h_{lk}\bar{L}_k H R_k + h_{dk}\bar{L}'_{qk} H R_{dk} + h_{uk}\bar{L}'_{qk}(i\sigma^2 H^*)R_{uk}] + h.c.,$$
$$\bar{L}'_{qk} = \begin{pmatrix} q_{ku} \\ q_{kd} \end{pmatrix}_L . \tag{53}$$

The potential term $V_0(H) = -M^2 H^+ H + \frac{\lambda}{2}(H^+ H)^2$ for $M^2 > 0$ gives rise to the spontaneous symmetry breaking. The doublet H acquires the nonzero vacuum expectation value

$$< H >= \begin{pmatrix} 0 \\ \frac{v}{\sqrt{2}} \end{pmatrix}, \tag{54}$$

where $v = 246$ GeV. In the unitary gauge, unphysical Goldstone massless fields are absent and the Higgs doublet scalar field depends on the single physical scalar field $h(x)$ (Higgs field):

$$H(x) = \begin{pmatrix} 0 \\ \frac{v}{\sqrt{2}} + \frac{h(x)}{\sqrt{2}} \end{pmatrix}. \tag{55}$$

Due to spontaneous gauge symmetry breaking gauge fields except photon field acquire masses. Diagonalization of mass matrix gives

$$W^\pm_\mu = \frac{1}{\sqrt{2}}(W^1_\mu \mp W^2_\mu),\ M_W = \frac{1}{2} g_2 v, \tag{56}$$

$$Z_\mu = \frac{1}{\sqrt{g_2^2 + g_1^2}}(g_2 W^3_\mu - g_1 W^0_\mu),\ M_Z = \frac{1}{2}\sqrt{g_2^2 + g_1^2}\, v, \tag{57}$$

$$A_\mu = \frac{1}{\sqrt{g_2^2 + g_1^2}}(g_1 W^3_\mu + g_2 W^0_\mu),\ M_A = 0, \tag{58}$$

where $W^\pm_\mu$, Z_μ are charged and neutral electroweak bosons, A_μ is photon. It is convenient to introduce rotation angle θ_W between (W^3, W^0) and (Z, A) which is called Weinberg angle

$$\sin\theta_W \equiv \frac{g_1}{\sqrt{g_1^2 + g_2^2}}. \tag{59}$$

Experimentally $\sin^2\theta_W \approx 0.23$ [11]. The formula for the electric charge e has the form

$$e = \frac{g_2 g_1}{\sqrt{g_2^2 + g_1^2}}. \tag{60}$$

At the tree-level the Higgs boson mass is determined by the formula

$$m_h = \sqrt{2}M = \sqrt{\lambda}v\,. \tag{61}$$

The Lagrangian L_{Yuk} is responsible for the fermion masses generation. In the unitary gauge the Lagrangian L_{HYM} takes the form

$$L_{HYM} = \frac{1}{2}\partial^\mu h \partial_\mu h + M_W^2(1+\frac{h}{v})^2 W_\mu^+ W^\mu + \frac{1}{2}M_Z^2(1+\frac{h}{v})^2 Z^\mu Z_\mu\,. \tag{62}$$

The Yukawa Lagrangian in the unitary gauge can be written in the form

$$L_{Yuk} = -\sum_i m_{\psi_i}(1+\frac{h}{v})\bar{\psi}_i\psi_i\,. \tag{63}$$

At present LEP1 lower bound on the Higgs boson mass is [12]

$$m_h > 63.5\,\mathrm{GeV}\,. \tag{64}$$

In standard Weinberg-Salam model there are several theoretical bounds on the Higgs boson mass:

(i) Tree-level unitarity requirement leads to $m_h \leq 1$ TeV [13].

(ii) The requirement of the absence of the Landau pole singularity for the effective Higgs self-coupling constant for energies up to 10^{14} GeV gives $m_h \leq 200$ GeV for $m_t \leq 200$ GeV [14].

(iii) The vacuum stability requirement leads to the lower bound on the Higgs boson mass which depends on the top-quark mass [15].

The renormalization group equations for the effective coupling constants in neglection of all Yukawa coupling constants except top-quark Yukawa coupling constant in one-loop approximation read

$$\frac{d\bar{g}_3}{dt} = -7\bar{g}_3^3\,, \tag{65}$$

$$\frac{d\bar{g}_2}{dt} = -(\frac{19}{6})\bar{g}_2^3\,, \tag{66}$$

$$\frac{d\bar{g}_1}{dt} = (\frac{41}{6})\bar{g}_1^3\,, \tag{67}$$

$$\frac{d\bar{h}_t}{dt} = (\frac{9\bar{h}_t^2}{2} - 8\bar{g}_3^2 - \frac{9\bar{g}_2^2}{4} - \frac{17\bar{g}_1^2}{12})\bar{h}_t\,, \tag{68}$$

$$\frac{d\bar{\lambda}}{dt} = 12(\bar{\lambda}^2 + (\bar{h}_t^2 - \frac{\bar{g}_1^2}{4} - \frac{3\bar{g}_2^2}{4})\lambda - \bar{h}_t^4 + \frac{\bar{g}_1^4}{16} + \frac{\bar{g}_1^2\bar{g}_2^2}{8} + \frac{3\bar{g}_2^4}{16})\,, \tag{69}$$

$$t = (\frac{1}{16\pi^2})\ln(\mu/m_Z)\,. \tag{70}$$

Here $\bar{g}_3$, $\bar{g}_2$ and $\bar{g}_1$ are the $SU_c(3)$, $SU_L(2)$ and $U(1)$ gauge couplings, respectively, and $\bar{h}_t$ is the top-quark Yukawa coupling constant. In our estimates we took $m_t^{pole} = 175$ GeV, $\bar{\alpha}_3(m_Z) = 0.118$, $\bar{\alpha}_{em}^{-1}(m_Z) = 127.9$, $\sin^2\theta_W(m_Z) = 0.2337$, $\alpha_i \equiv \frac{g_i^2}{4\pi}$. From the requirement of the absence of Landau pole singularity for the Higgs self-coupling constant λ for the scales up to $\Lambda = (10^3; 10^4; 10^6; 10^8; 10^{10}; 10^{12}; 10^{14})$ GeV (to be precise we require that at the scale Λ the Higgs self-coupling constant is $\frac{\bar{\lambda}^2(\Lambda)}{4\pi} \leq 1$) we have found the upper bound on the Higgs boson mass $m_h \leq$ (400; 300; 240; 200; 180; 170; 160) GeV, respectively. Roughly speaking, the vacuum stability bound comes from the requirement that the Higgs self-interaction coupling is nonnegative $\bar{\lambda}(\mu) \geq 0$ for the scales $\mu \leq M_s$. Here M_s is the scale up to which the standard model is applicable. Suppose that at scales up to M_s standard model works and at scales $M \geq M_s$ we have some supersymmetric extension of the standard model. It should be noted that the most popular at present the minimal supersymmetric standard model (MSSM) predicts that the effective Higgs self-coupling constant for the standard model at the scale of supersymmetry breaking M_s has to obey the inequality

$$0 \leq \bar{\lambda}(M_s) = (\bar{g}_1^2(M_s) + \bar{g}_2^2(M_s))(\cos(2\varphi))^2/4 \leq (\bar{g}_1^2(M_s) + \bar{g}_2^2(M_s))/4\,. \quad (71)$$

So the assumption that the standard Weinberg-Salam model originates from its supersymmetric extension with the supersymmetry broken at scale M_s allows us to obtain nontrivial information about the low energy effective Higgs self-coupling constant in the effective potential $V = -M^2H^+H + \frac{\lambda}{2}(H^+H)^2$ and hence to obtain nontrivial information about the Higgs boson mass. It should be noted that in nonminimal supersymmetric electroweak models, say in the model with additional gauge singlet σ, we have due to the $k\sigma H_1 i\tau_2 H_2$-term in the superpotential an additional term $k^2|H_1 i\tau_2 H_2|^2$ in the potential and as a consequence our boundary condition for the Higgs self-coupling constant has to be modified, namely

$$\bar{\lambda}(M_s) = \frac{1}{4}(\bar{g}_1^2(M_s) + \bar{g}_2^2(M_s))\cos^2(2\varphi) + \frac{1}{2}\bar{k}^2(M_s)\sin^2(2\varphi) \geq 0\,. \quad (72)$$

The boundary condition (72) depends on unknown coupling constant $\bar{k}^2(M_s)$. However it is very important to stress that for all nonminimal supersymmetric models broken to standard Weinberg-Salam model at scale M_s the effective Higgs self-coupling constant $\bar{\lambda}(M_s)$ is nonnegative which is a direct consequence of the nonnegativity of the effective potential in supersymmetric models. Therefore the vacuum stability requirement results naturally [16] if supersymmetry is broken at some high scale M_s and at lower scales the standard Weinberg-Salam model is an effective theory. For MSSM with boundary condition (71) for the Higgs self-coupling constant $\bar{\lambda}(M_s)$ we have integrated numerically renormalization group

equations in two-loop approximation. Also we took into account the one-loop correction to the Higgs boson mass (running Higgs boson mass $\bar{m}_h(\mu) = \sqrt{\bar{\lambda}(\mu)}v$ does not coincide with pole Higgs boson mass). Our results for the Higgs boson mass for different values of M_s and m_t^{pole} are presented in the Table. Here $k = 0$ corresponds to the boundary condition $\bar{\lambda}(M_s) = 0$, and $k = 1$ corresponds to the boundary condition $\bar{\lambda}(M_s) = \frac{1}{4}(\bar{g}_1^2 + \bar{g}_2^2)$.

Table. The dependence of the Higgs boson mass on the values of M_s, m_t^{pole} and $k = 0, 1$. Everything except k is in GeV

m_t^{pole}	165	165	170	170	175	175	180	180	185	185
	k=0	k=1	k=0	k=1	k=0	k=1	k=0	k=1	k=0	k=1
$M_s = 10^3$	69	111	74	114	78	117	83	120	88	123
$M_s = 10^{3.5}$	81	117	86	120	92	124	98	128	104	132
$M_s = 10^4$	89	121	95	125	101	130	108	134	114	139
$M_s = 10^6$	105	129	113	135	121	141	129	147	137	153
$M_s = 10^8$	112	132	120	138	129	147	138	152	146	159
$M_s = 10^{10}$	115	133	124	140	133	147	142	154	151	161
$M_s = 10^{12}$	117	134	126	141	136	147	145	154	154	161
$M_s = 10^{14}$	118	134	127	141	132	148	147	156	156	164
$M_s = 10^{16}$	118	134	128	141	138	148	148	156	158	164

The tree-level Higgs boson couplings to gauge bosons and fermions can be deduced from the Lagrangians (62, 63). Of these, the hW^+W^-, hZZ and $h\bar{\psi}\psi$ are the most important for the phenomenology. The partial decay width into fermion-antifermion pair is [10]

$$\Gamma(h \to \psi\bar{\psi}) = \frac{G_F m_\psi^2 m_h N_c}{4\pi\sqrt{2}}(1 - \frac{4m_\psi^2}{m_h^2})^{\frac{3}{2}}, \tag{73}$$

where N_c is the number of fermion colours. For $m_h \leq 2m_W$ Higgs boson decays mainly with ≈ 90 per cent probability into b-quark-antiquark pair and with ≈ 10 per cent probability into τ lepton-antilepton pair. An account of higher order QCD corrections can be effectively taken into account in the formula (73) for the Higgs boson decay into b-quark-antiquark pair by the replacement of pole b-quark mass in formula (73) by the effective b-quark mass $\bar{m}_b(m_h)$. Higgs boson with $m_h \geq 2M_W$ will decay into pairs of gauge bosons with the partial widths

$$\Gamma(h \to W^+W^-) = \frac{G_F m_h^3}{32\pi\sqrt{2}}(4 - 4a_w + 3a_w^2)(1 - a_w)^{\frac{1}{2}}, \tag{74}$$

$$\Gamma(h \to Z^0Z^0) = \frac{G_F m_h^3}{64\pi\sqrt{2}}(4 - 4a_Z + 3a_Z^2)(1 - a_Z)^{\frac{1}{2}}, \tag{75}$$

where $a_W = \frac{4M_W^2}{m_h^2}$ and $a_Z = \frac{4M_Z^2}{m_h^2}$. In the heavy Higgs mass regime ($2m_Z \leq m_h \leq 800$ GeV), the Higgs boson decays dominantly into gauge bosons. For example, for $m_h \gg 2m_Z$ one can find that

$$\Gamma(h \to W^+W^-) = 2\Gamma(h \to ZZ) \simeq \frac{G_F m_h^3}{8\pi\sqrt{2}}. \tag{76}$$

The m_h^3 behaviour is a consequence of the longitudinal polarization states of the W and Z. As m_h gets large, so does the coupling of h to the Goldstone bosons which have been eaten by the W and Z. However, the Higgs boson decay width to a pair of heavy quarks growth only linearly in the Higgs boson mass. Thus, for the Higgs masses sufficiently above $2m_Z$, the total Higgs boson width is well approximated by ignoring the Higgs decay to $t\bar{t}$ and including only the two gauge boson modes. For heavy Higgs boson mass one can find that

$$\Gamma_{total}(H) \simeq 0.48 \text{ TeV}(\frac{m_h}{1 \text{ TeV}})^3. \tag{77}$$

It should be noted that there are a number of Higgs couplings which are absent at tree level but appear at one-loop level. Among them the couplings of the Higgs boson to two gluons and two photons are extremely important for the Higgs boson searches at supercolliders. One-loop induced Higgs coupling to two gluons is due to t-quark exchange in the loop [17] and it leads to an effective Lagrangian

$$L_{hgg}^{eff} = \frac{g_2\alpha_s}{24\pi m_W} h G_{\mu\nu}^a G^{a\mu\nu}. \tag{78}$$

Using the effective Lagrangian (78) one can find that

$$\Gamma(h \to gg) = \frac{g_2^2\alpha_s^2 m_h^3}{288\pi^3 m_W^2}. \tag{79}$$

Also very important is the one-loop induced Higgs boson coupling to two photons due to W- and t-quark exchanges in the loop. The corresponding expression for the decay width of the Higgs boson into two photons is contained in [18].

Consider now the Higgs boson search at supercolliders. For completeness let us start with LEP2. At LEP2 with the total energy $\sqrt{s} = 192$ GeV the dominant Higgs production process is $e^+e^- \to hZ$. The corresponding cross section at tree level is given by [19]

$$\sigma(e^+e^- \to hZ) = \frac{\pi\alpha^2\lambda^{1/2}(\lambda + 12sM_Z^2)[1 + (1 - 4\sin^2\theta_W)^2]}{192s^2\sin^4\theta_W\cos^4\theta_W(s - M_Z^2)^2}, \tag{80}$$

where $\lambda \equiv (s - m_h^2 - M_Z^2)^2 - 4m_h^2M_Z^2$. One can see that for a fixed value of m_h, the cross section is maximal for $\sqrt{s} \approx m_Z + \sqrt{2}m_h$. For $L_t = 500\ pb^{-1}$

one expects to observe the Higgs bosons using the signature $Z \to \nu\bar{\nu}$, $h \to b\bar{b}$ for masses up to M_Z. Note that the region $m_h \simeq M_Z$ is particularly troublesome due to the $e^+e^- \to ZZ$ background. Both ZZ and hZ lead to four-fermion states. However, these can be separated by making use of the fact that $Br(h \to b\bar{b}) \approx 90$ per cent as compared with $Br(Z \to b\bar{b}) \approx 20$ per cent. Given sufficient energy and luminosity, and a vertex detector that can tag b-quark jets with high efficiency, it would be possible to discover a Higgs boson if it is degenerate in mass with Z-boson.

At LHC the dominant mechanism for the Higgs boson production is gluon-gluon fusion. Also WW fusion becomes important for heavy Higgs boson. The cross section for the Higgs boson production due to gluon-gluon fusion has the form

$$\frac{d\sigma}{dy}(AB \to h + X) = \frac{\pi^2 \Gamma(h \to gg)}{8 m_h s} G_A(x_a, m_h^2) G_B(x_b, m_h^2) , \tag{81}$$

where G_A and G_B are the gluon distributions functions in hadrons A and B, respectively, and

$$x_a = \frac{m_h e^y}{\sqrt{s}}, \; x_b = \frac{m_h e^{-y}}{\sqrt{s}} , \tag{82}$$

$$y = \frac{1}{2} \ln \left(\frac{E_h + p_{3h}}{E_h - p_{3h}} \right) . \tag{83}$$

The rapidity y is defined in terms of the Higgs boson energy and longitudinal momentum, defined in the laboratory frame.

3.2.3. Search for Standard Higgs Boson at CMS

The Search for $h \to \gamma\gamma$. One of the most important reactions for the search for Higgs boson at LHC is

$$pp \to (h \to \gamma\gamma) + \ldots , \tag{84}$$

which is the most promising one for the search for Higgs boson in the most interesting region 90 GeV$\leq m_h \leq$140 GeV.

The key features that enable CMS detector to obtain clear two-photon mass peaks, significantly above background throughout the intermediate mass range, are:

i. An electromagnetic calorimeter with an excellent energy resolution (this requires calibration to high precision, which in turn requires a good inner tracking system).

ii. A large acceptance (the precision electromagnetic calorimetry extends to $|\eta| = 2.5$), adequate neutral pion rejection and (at high luminosity) a good

measurement of photon direction. This requires fine lateral segmentation and a preshower detector.

iii. Use of powerful inner tracking system for isolation cuts.

The cross section times branching has been estimated to be $\sigma Br(h \to \gamma\gamma) = 76fb(68fb)$ for $m_h = 110(130)$ GeV, the uncertainty in the cross section calculation is (30 - 50) per cent. The imposition of cuts ($|\eta| \leq 2.5$, $p_T^{\gamma_1} \geq 40$ GeV, $p_T^{\gamma_2} \geq 25$ GeV) allows one to decrease the background in a reasonable magnitude. The jet background is reduced by imposing an isolation cut, which also reduces the bremsstrahlung background. Photon is defined to be isolated if there is no charged track or electromagnetic shower with a momentum greater than 2.5 GeV within a region $\Delta R \leq 0.3$ around it. The photons from the decay of π^0 of the relevant transverse momenta are separated in the calorimeter by a lateral distance of the order of 1 cm. An efficiency of 64 per cent was assumed for reconstruction of each photon (i.e., 41 per cent per event). The crystal calorimeter was assumed to have an energy resolution $\Delta E/E = 0.02/\sqrt{E} \oplus 0.005 \oplus 0.2/E$ in the barrel and $\Delta E/E = 0.05/\sqrt{E} \oplus 0.005 \oplus 0.2/E$ in the endcap, where there is a preshower detector. At high luminosity, a barrel preshower detector covers $|\eta| < 1.1$, resulting in a resolution $\Delta E/E = 0.05/\sqrt{E} \oplus 0.005 \oplus 0.2/E$ and an ability to measure the photon direction with resolution $\Delta\alpha = 40$ mrad$/\sqrt{E}$ in this region.

The background to the $h \to \gamma\gamma$ may be divided into 3 categories:

1. prompt diphoton production from quark annihilation and gluon fusion diagrams — irreducible background,

2. prompt diphoton production from bremsstrahlung from the outgoing quark line in the QCD Compton diagram,

3. background from jets, where an electromagnetic energy deposit originates from the decay of neutral hadrons in a jet from 1 jet + 1 prompt photon.

The signal significance $\sigma = \frac{N_S}{\sqrt{N_B}}$ is estimated to be $7\sigma(9\sigma)$ for $m_h = 110(130)$GeV and for low luminosity $L_{low,t} = 3 \cdot 10^4 \text{pb}^{-1}$ and $10\sigma(13\sigma)$ for $m_h = 110(130)$ GeV and for high luminosity $L_{high,t} = 10^5 \text{pb}^{-1}$. The general conclusion is that at 5σ level it would be possible to discover Higgs boson for 95 GeV$\leq m_h \leq$ 145 GeV at low luminosity and at high luminosity the corresponding Higgs boson mass discovery interval is 85 GeV$\leq m_h \leq$ 150 GeV.

Search for $h \to \gamma\gamma$ in Association with High E_T Jets. The possibility of the search for $h \to \gamma\gamma$ with large E_T-jet allows one to improve $signal/background$ ratio. There are several sources of such Higgs + jet events. One is the next to leading order corrections to $gg \to h$ with hard gluons. Others are the associated production of $\bar{t}th, Wh, Zh$ and the WW- and Zh-fusion mechanisms.

The cuts that provide optimal sensitivity are [1]:

i. Two isolated photons are required, with $p_t^{\gamma_1} \geq 40$ GeV and $p_t^{\gamma_2} \geq 60$ GeV, $|\eta| \leq 2.5$ and $p_t^{\gamma\gamma} \geq 50$ GeV.

ii. Number of jets ≥ 2, $E_t^{jet} \geq 40$ GeV for the central jets ($|\eta| \leq 2.4$) and $E^{jet} \geq 800$ GeV for the forward ones ($2.4 \leq |\eta| \leq 4.6$).

iii. Photons are isolated with no charged or neutral particles with $p_t \geq 2$ GeV within a cone $\Delta R \leq 0.3$ around each photon's direction.

iiii. γ-jet isolation $\Delta R(\gamma, jet) > 1.5$ (to suppress the bremsstrahlung contribution).

The calculations give encouraging results, namely for $L_{high,t} = 1.6 \cdot 10^5 \mathrm{pb}^{-1}$ it would be possible to discover the Higgs boson for 70 GeV$\leq m_h \leq$150 GeV with $\geq 7\sigma$ signal significance. Note that the background is not only much smaller in magnitude than in the inclusive $h \to \gamma\gamma$ search, but it is also peaked at higher masses, away from the most difficult region $m(\gamma\gamma) \leq 90$ GeV.

$h \to \gamma\gamma$ **in Associated** Wh **and** $\bar{t}th$**-Production.** The $Wh \to l\gamma\gamma + X$ and $\bar{t}th \to l\gamma\gamma + X$ final states are other promising signature for the Higgs boson search. The production cross section is smaller than the inclusive $h \to \gamma\gamma$ by a factor of ≈ 30. However the isolated hard lepton from the W- and t-decay allows one to obtain a strong background reduction and to indicate the primary vertex at any luminosity. The main backgrounds are: $W\gamma\gamma$, $W\gamma + jet$, $W + 2jets$, $t\bar{t}\gamma\gamma$, $t\bar{t}\gamma$, $t\bar{t}$, $b\bar{b}$, $c\bar{c}$ and $t\bar{b}$, with a real lepton in the final state and one or two jets faking photons due to hard bremsstrahlung. For 80 GeV$\leq m_h \leq$120 GeV and $L_{high,t} = 1.6 \cdot 10^5 \mathrm{pb}^{-1}$ the signal significance is better than 6σ [1].

$h \to ZZ^*(ZZ) \to 4$ **Leptons.** The search for the standard Higgs boson using the reaction $h \to ZZ^*(ZZ) \to 4$ leptons is possible for a broad mass range 130 GeV$\leq m_h \leq$800 GeV. Below $2M_Z$ the event rate is small and the background reduction is more difficult, as one of the Zs is off mass shell. In this mass region the width of the Higgs boson is small $\Gamma_h < 1$ GeV. The significance of the signal is proportional to the mass resolution, so the lepton momentum resolution is of decisive importance. The geometrical and kinematic acceptance for leptons is also very important in these channels [1] in the $m_h < 2M_Z$ mass region , the main backgrounds are from $t\bar{t}$, $Zb\bar{b}$ and ZZ^*. The ZZ^* background is irreducible and peaks sharply near the ZZ threshold. The $Zb\bar{b}$ background cannot be reduced by a Z mass cut, but it can be suppressed by lepton isolation. The $t\bar{t}$ background can be reduced by a Z mass cut and by isolation cuts. The standard event cuts were chosen the following [1]: one electron with $p_t > 20$ GeV; one with $p_t > 15$ GeV, and the remaining two electrons with $p_t > 10$ GeV, all within $|\eta| < 2.5$. For muons, the corresponding p_t cuts are 20, 10 and 5 GeV in the rapidity range $|\eta| < 2.4$. For $m_h = 130$ GeV the overall (kinematic and geometrical) acceptance for the four-electron channel is 22 per cent; and for the four-muon channel, 42 per cent. For $m_h = 170$ GeV these acceptances increase to 38 per cent and 48 per cent, respectively. To select $h \to ZZ^*$ events and suppress the large $t\bar{t}$ background, one of the e^+e^- or $\mu^+\mu^-$ pairs was assumed to be within $\pm 2\sigma_Z$ of the Z mass. There is a fraction of events where both Zs are off-shell. This effect results in a 24 per cent loss for $m_h = 130$ GeV, decreasing

to 12 per cent for $m_h = 170$ GeV. The M_Z cut reduces $t\bar{t}$ background by a factor of 11 in the $Z \to \mu^+\mu^-$ channel and by a factor of 5 in the $Z \to e^+e^-$ channel. For two softer leptons, $M(ll) > 12$ GeV is also required.

For the region 130 GeV$\leq m_h \leq$180 GeV it would be possible for $L_{high,t} = 10^5 \text{pb}^{-1}$ to discover the Higgs boson with $\geq 5\sigma$ signal significance except narrow mass region around 170 GeV. For $m_h \geq 180$ GeV the $h \to ZZ \to 4l^{\pm}$ channel is sensitive for low luminosity 10^4pb^{-1} from $2m_Z$ to 400 GeV. The main background here is nonresonant ZZ-production. The conclusion is that even at low luminosity $L_{low,t} = 10^4 \text{pb}^{-1}$ it would be possible to discover Higgs boson for $2m_Z \leq m_h \leq 400$ GeV [1].

The Use of Channels $h \to ll\nu\nu$, $h \to WW \to l\nu jj$ and $h \to ZZ \to lljj$. The channel $h \to ll\nu\nu$ has a six times larger branching than $h \to 4l^{\pm}$. The main background comes from ZZ, ZW, $t\bar{t}$ and $Z + jets$. The chosen cuts are the following:

1. $E_t^{miss} \geq 100$ GeV.
2. Two leptons are required, with $p_t \geq 20$ GeV, $|\eta| \leq 1.8$, and $p_t^{ll} \geq 60$ GeV.
3. $|M_Z - M_{ll}| \leq 6$ GeV.
4. No other isolated leptons with $p_t \geq 6$ GeV.
5. No central jets with $E_t \geq 150$ GeV.
6. No jets back-to-back with leptons (cosine of the angle between the momentum of the lepton pair and sum of the momenta of the jets is ≥ -0.8).
7. E_t^{miss} vector back-to-back with the lepton pair (cosine of the angle in the transverse plane between the two-lepton momentum and the missing transverse momentum ≤ 0.8).

The conclusion is that using this mode it would be possible to discover Higgs boson in the interval 400 GeV$\leq m_h \leq$(800 - 900) GeV [1].

The channels $h \to WW \to l\nu jj$ and $h \to ZZ \to lljj$ are important in the $m_h \approx 1$ TeV mass range, where the large $W, Z \to q\bar{q}$ branching ratios must be used. Also high lepton pairs with $m_{ll} \approx M_Z$ for $h \to ZZ$ or a high p_t lepton pair plus large E_t^{miss} for $h \to WW$ must be used. In addition, two hard jets from the hadronic decays of Z/W with $m_{jj} \approx M_{Z/W}$ are required. The backgrounds are: $Z + jets$, ZW, WW, $t\bar{t}$, WW, WZ. For $m_h \approx 1$ TeV the Higgs boson is very broad ($\Gamma_h \approx 0.5$ TeV and WW/ZZ fusion mechanism represents about 50 per cent of the total production cross section), therefore forward-region signature is essential. The appropriate cuts are the following:

i. $E_t^{miss} \geq 150$ GeV, $p_t^l \geq 150$ GeV, $p_t^W \geq 300$ GeV for $h \to WW$, or $p_t^l \geq 50$ GeV, $p_t^Z \geq 50$ GeV, $p_t^Z \geq 150$ GeV, $|m_Z - m_{ll}| \leq 10$ GeV for $h \to ZZ$.

ii. $|m_{jj} - m_{W/Z}| \leq 15$ GeV for the central jet pair.

iii. $E_t^{jet} \geq 10$ GeV, $E^{jet} \geq 400$ GeV, $|\eta| \geq 2.4$ for the two forward tagging jets.

The main conclusion is that the use of the reactions $h \to WW \to l\nu jj$ and

$h \to ZZ \to lljj$ allows one to discover the heavy Higgs boson with a mass up to 1 TeV for $L_{high,t} = 10^5 \text{pb}^{-1}$ [1].

3.2.4. B-Physics in SM

General Comments. The main task of B-physics investigation at LHC is the observation of CP-violation. For such a measurement high statistics are important since the useful decay rates have branchings $(10^{-4} - 10^{-7})$. At LHC $(10^{12} - 10^{13})$ $b\bar{b}$-pairs will be produced per year so the main problem here is to trigger and select the interesting modes. The violation of CP-symmetry is one of the most intriguing aspects of high-energy physics. At present there is only a single measurement of a CP-violation parameter: the measurement of ϵ_K in K-decays. The standard model description of CP-violation is very predictive — all CP-violating effects are related to the phase δ of the Cabibbo–Kobayashi–Maskawa (CKM) matrix. Note that in standard model also θ-term

$$\theta \frac{\alpha_s}{4\pi} Tr G_{\mu\nu} \tilde{G}^{\mu\nu} \tag{85}$$

in QCD Lagrangian violates CP-symmetry [20]. θ-term gives nonzero contribution to electric dipole moment of the neutron [20]. The current experimental bound on the electric dipole moment of the neutron $|d_n| \leq 1.1 \cdot 10^{-25} e \cdot \text{cm}$ implies that $|\theta| \leq 10^{-9}$ that corresponds to an extreme fine-tuning of a parameter θ of the QCD Lagrangian. Therefore there are good prospects that detailed investigation of CP-violation in B-decays will provide us important information on the possible mechanisms of CP-violation.

Let us start with brief description of P-, C- and CP-transformations [21]. The parity transformation is a space-time transformation, under which $t \to -t$ and $\vec{x} \to -\vec{x}$. It changes the sign of momenta, $\vec{p} \to -\vec{p}$, leaving spins unchanged. For pseudoscalar mesons P and $\tilde{P}$, the parity transformation could be defined as

$$\hat{P}|P(\vec{p})> = -|P(-\vec{p})>, \tag{86}$$

$$\hat{P}|\tilde{P}(\vec{p})> = -|\tilde{P}(-\vec{p})> . \tag{87}$$

Charge conjugation relates particles and antiparticles, leaving all space-time coordinates unchanged, i.e.,

$$\hat{C}|P(\vec{p})> = |\tilde{P}(\vec{p})>, \tag{88}$$

$$\hat{C}|\tilde{P}(\vec{p})> = |P(\vec{p})> . \tag{89}$$

The combined CP-transformation acts on pseudoscalar mesons in the following way:

$$\hat{C}\hat{P}|P(\vec{p})> = -|\tilde{P}(-\vec{p})>, \tag{90}$$

$$\hat{C}\hat{P}|\tilde{P}(\vec{p})>=-|P(-\vec{p})>\ . \tag{91}$$

For neutral P^0- and $\tilde{P}^0$-mesons one can construct the CP-eigenstates

$|P_1^0>=\frac{1}{\sqrt{2}}(|P^0>-|\tilde{P}^0>)$,
$|P_2^0>=\frac{1}{\sqrt{2}}(|P^0>+|\tilde{P}^0>)$,
which obey

$\hat{C}\hat{P}|P_1^0>=|P_1^0>$,
$\hat{C}\hat{P}|P_2^0>=-|P_2^0>$.

CP-Violation in Standard Model. The standard model gauge group $SU_C(3)\otimes SU_L(2)\otimes U(1)$ is spontaneously broken to $SU_C(3)\otimes U(1)$ due to nonzero vacuum expectation value of the Higgs doublet. This gives the masses to the W- and Z-bosons, as well as to the quarks and leptons. The quark masses arise from the Yukawa couplings to the Higgs doublet. The Yukawa interactions are written in terms of the weak eigenstates $q^{'}$ of the quark fields. After the electroweak symmetry breaking the quark fields are redefined so as to obtain the mass terms in the canonical way. In the weak basis these charged-current interactions have the form

$$L_{int}=-\frac{g_2}{\sqrt{2}}(\bar{u}_L^{'},\bar{c}_L^{'},\bar{t}_L^{'})\gamma^\mu\begin{pmatrix} d_L^{'} \\ s_L^{'} \\ b_L^{'}\end{pmatrix}W_\mu^+ + h.c.\,. \tag{92}$$

In terms of the mass eigenstates q the L_{int} can be rewritten in the form

$$L_{int}=-\frac{g_2}{\sqrt{2}}(\bar{u}_L,\bar{c}_L,\bar{t}_L)\gamma^\mu V_{CKM}\begin{pmatrix} d_L \\ s_L \\ b_L\end{pmatrix}W_\mu^+ + h.c.\,. \tag{93}$$

The CKM mixing matrix $V_{\rm CKM}$ is a unitary matrix in flavour space. In the case of three generations, $V_{\rm CKM}$ can be parametrized by three Euler angles and six phases, five of which can be removed by redefinition of the left-handed quark fields. So three angles θ_{ij} and one observable complex phase δ remain in the quark mixing matrix [21].

The "standard parametrization" of the CKM matrix is

$$V_{CKM}=\begin{pmatrix} c_{12}c_{13} & s_{12}c_{13} & s_{13}e^{-i\delta} \\ -s_{12}c_{23}-c_{12}s_{23}s_{13}e^{i\delta} & c_{12}c_{23}-s_{12}s_{23}s_{13}e^{i\delta} & s_{23}c_{13} \\ s_{12}s_{23}-c_{12}c_{23}s_{13}e^{i\delta} & -c_{12}s_{23}-s_{12}c_{23}s_{13}e^{i\delta} & c_{23}c_{13}\end{pmatrix}. \tag{94}$$

Here $c_{ij}=\cos(\theta_{ij})$ and $s_{ij}=\sin(\theta_{ij})$. The imaginary part of the mixing matrix is necessary to describe CP-violation in standard model. In general CP is violated

in flavour changing decays if there is no degeneracy of any two quark masses and if the quantity $J_{CP} \neq 0$, where

$$J_{CP} = |Im(V_{ij}V_{kl}V_{il}^{*}V_{kj}^{*}|;\ i \neq k\ j \neq l\,. \tag{95}$$

It can be shown that all CP-violating amplitudes in the standard model are proportional to J_{CP}.

For many applications it is more convenient to use an approximate parametrization of the CKM matrix (Wolfenstein parametrization) [22]

$$V_{\mathrm{CKM}} \simeq \begin{pmatrix} 1-\frac{\lambda^2}{2} & \lambda & A\lambda^3(\rho - i\eta) \\ -\lambda & 1-\frac{\lambda^2}{2} & A\lambda^2 \\ A\lambda^3(1-\rho-i\eta) & -A\lambda^2 & 1 \end{pmatrix} + O(\lambda^4)\,. \tag{96}$$

One can find that

$$J_{CP} \simeq A^2\eta\lambda^6 \simeq 1.1 \cdot 10^{-4} \cdot A^2\eta\,. \tag{97}$$

The two Wolfenstein parameters λ and A are experimentally well determined [23]

$$\lambda = |V_{us}| = 0.2205 \pm 0.0018\,, \tag{98}$$

$$A = |\frac{V_{cb}}{V_{us}^2}| = 0.80 \pm 0.04\,. \tag{99}$$

A simple way to take into account the implications of the CKM matrix unitarity is provided by the so-called unitarity triangle which uses the fact that the unitarity equation

$$V_{ij}V_{ik}^{*} = 0\ (j \neq k) \tag{100}$$

can be represented as the equation of a closed triangle in the complex plane. There are six such triangles with the same area [24]

$$|A_{\Delta}| = \frac{1}{2}J_{CP}\,. \tag{101}$$

Most useful from the phenomenological point of view is the triangle relation

$$V_{ud}V_{ub}^{*} + V_{cd}V_{cb}^{*} + V_{td}V_{tb}^{*} = 0\,, \tag{102}$$

which determines the triangle with the angles α, β, γ ($\alpha + \beta + \gamma = \pi$). The present fit to data for triangle gives: $\sin(2\alpha) \approx 0.7$, $\sin(2\beta) \approx 0.5$, $\sin(\gamma) \approx 0.9$.

Direct CP-Violation in Weak Decays. Consider two decay processes related to each other by a CP-transformation. Let P and $\tilde{P}$ be CP-conjugated pseudoscalar meson states, and f and $\tilde{f}$ some CP-conjugated final states:

$$\hat{C}\hat{P}|P> = e^{i\phi_P}|\tilde{P}>,\ \hat{C}\hat{P}|f> = e^{i\phi_f}|\tilde{f}>\,. \tag{103}$$

The phases ϕ_P and ϕ_f are arbitrary. The CP-conjugated amplitudes , A and $\bar{A}$, can be written as

$$A =< f|H|P >= \sum_i A_i e^{i\delta_i} e^{i\phi_i} , \tag{104}$$

$$\bar{A} =< \tilde{f}|H|\tilde{P} >= e^{i(\phi_P - \phi_f)} \sum_i A_i e^{i\delta_i} e^{-i\phi_i} , \tag{105}$$

where H is the effective Hamiltonian for weak decays, and A_i are real partial amplitudes. The weak phases ϕ_i are parameters of the CP-violating Lagrangian. They appear in the electroweak sector of the theory and enter a and $\bar{A}$ with opposite signs. The strong phases δ_i appear in scattering amplitudes even if the Lagrangian is CP-invariant and they enter A and $\bar{A}$ with the same sign. It appears that the ratio

$$|\frac{\bar{A}}{A}| = |\frac{\sum_i A_i e^{i\delta_i} e^{i\phi_i}}{\sum_i A_i e^{i\delta_i} e^{-i\phi_i}}| \tag{106}$$

is independent of phase conventions. The nonequality

$$|\frac{\bar{A}}{A}| \neq 1 \tag{107}$$

implies direct CP-violation which comes from the interference of decay amplitudes leading to the same final states, that requires at least two partial amplitudes that differ in both the weak and strong phases.

Since the mixing is unavoidable in neutral meson decays, the best way to observe direct CP-violation are the decays of charged mesons. The CP-asymmetry is defined in a standard way:

$$a_f = \frac{\Gamma(P^+ \to f) - \Gamma(P^- \to \bar{f})}{\Gamma(P^+ \to f) + \Gamma(P^- \to \bar{f})} = \frac{1 - |\frac{\bar{A}}{A}|^2}{1 + |\frac{\bar{A}}{A}|^2} . \tag{108}$$

We have to consider nonleptonic decays since leptonic and semileptonic decays are usually dominated by a single diagram and complex phases cancel. Nonleptonic decays can receive both tree and penguin contributions [25]. Penguin diagrams typically involve other weak phases than tree diagrams. To get large interference effects one needs partial amplitudes with similar amplitude. Therefore it is necessary to look for decays in which tree contribution is suppressed by small CKM parameters that compensates the loop suppression of penguin diagrams. Another possibility is to consider tree forbidden decays, which can only proceed through penguin diagrams. Examples are $B^\pm \to K^\pm K$, $B^\pm \to K^\pm \phi$, $B^\pm \to K^{*\pm}\gamma$, $B^\pm \to \rho^\pm \gamma$. At present there is no experimental evidence for direct CP-violation.

Indirect CP-Violation in the Mixing of Neutral Mesons. The neutral mesons P^0 and $\tilde{P}^0$ can mix via common decay channels:

$$P^0 \leftrightarrow X \leftrightarrow \tilde{P}^0 \,. \tag{109}$$

An arbitrary neutral meson state can be written as a superposition of the eigenstates $a|P^0> + b|\tilde{P}^0>$ which obey Schrödinger equation

$$i\frac{d(a,b)}{dt} = \vec{H}(a,b) = (\vec{M} - \frac{i}{2}\vec{\Gamma})(a,b)\,, \tag{110}$$

where $\vec{M}$ and $\vec{\Gamma}$ are Hermitian 2×2 matrices. Since the Hamiltonian operator, $\vec{H}$, is not Hermitian, its eigenstates

$$|P_{1,2}> = p|P^0> \pm q|\tilde{P}^0>;\ |p^2| + |q^2| = 1 \tag{111}$$

are not orthogonal, and the eigenvalues

$$\mu_j = M_j - \frac{i}{2}\Gamma_j;\ j = 1,2 \tag{112}$$

are complex. The time evolution of the states P_i is given by

$$|P_i(t)> = e^{-iM_i t}e^{-\frac{1}{2}\Gamma_i t}|P_i(0)> \,. \tag{113}$$

One can show that the ratio

$$|\frac{q}{p}|^2 = |\frac{M_{12}^* - \frac{i}{2}\Gamma_{12}^*}{M_{12} - \frac{i}{2}\Gamma_{12}}|^2 \tag{114}$$

is independent of phase conventions. The condition $|\frac{q}{p}| \neq 1$ implies CP-violation due to the fact that flavour eigenstates are different from the CP-eigenstates. The following relations are valid:

$$(\Delta m)^2 - \frac{1}{4}(\Delta\Gamma)^2 = 4|M_{12}|^2 - |\Gamma_{12}|^2\,, \tag{115}$$

$$\Delta m \cdot \Delta\Gamma = 4Re(M_{12}\Gamma_{12}^*)\,, \tag{116}$$

$$\frac{q}{p} = -\frac{1}{2}\frac{\Delta m - \frac{i}{2}\Delta\Gamma}{M_{12} - \frac{i}{2}\Gamma_{12}} = -2\frac{M_{12}^* - \frac{i}{2}\Gamma_{12}^*}{\Delta m - \frac{i}{2}\Delta\Gamma}\,, \tag{117}$$

where $\Delta m = m_2 - m_1$ and $\Delta\Gamma = \Gamma_2 - \Gamma_1$. An alternative notation is defined $\tilde{\epsilon}$ such that

$$p = \frac{1+\tilde{\epsilon}}{\sqrt{2(1+|\tilde{\epsilon}|^2)}},\ q = \frac{1-\tilde{\epsilon}}{\sqrt{2(1+|\tilde{\epsilon}|^2)}},\ \frac{q}{p} = \frac{1-\tilde{\epsilon}}{1+\tilde{\epsilon}}\,. \tag{118}$$

Consider at first kaon system. Define the "short-lived" and "long-lived" neutral kaon states as $K_S = K_1$ and $K_L = K_2$. Experimentally,

$$\Delta m_K = m_L - m_S = (3.510 \pm 0.018) \times 10^{-15}\text{GeV}\,, \tag{119}$$

$$\Delta\Gamma_K = \Gamma_L - \Gamma_S = -(7.361 \pm 0.010) \times 10^{-15}\text{GeV}\,. \tag{120}$$

Define

$$\frac{\Gamma_{12}^*}{M_{12}^*} = -|\frac{\Gamma_{12}}{M_{12}}|e^{i\varphi_{12}}\,. \tag{121}$$

From the last definition we find that

$$|\frac{q}{p}|_K - 1 \simeq -2Re(\tilde{\epsilon}_K) \simeq -\varphi_{12} = O(10^{-3})\,. \tag{122}$$

For B-meson systems decay channels common to B^0 and $\tilde{B}^0$, which are responsible for the difference $\Delta\Gamma_B$, are known to have branching ratios of the order of 10^{-3} or less. Hence $|\frac{\Delta\Gamma_B}{\Gamma_B}| \leq O(10^{-2})$. The observed $B^0 - \tilde{B}^0$ mixing implies $\Delta m_B/\Gamma_B = 0.74 \pm 0.04$ that means $|\Delta\Gamma_B| \ll \Delta m_B$. Therefore, the lifetime difference between the CP-eigenstates is very small and it is possible to define these states as "light" and "heavy", $B_L = B_1$ and $B_H = B_2$. It follows that $|\Gamma_{12}| \ll |M_{12}|$, and to the first order in Γ_{12}/M_{12} one can find that

$$|\frac{q}{p}|_B - 1 \simeq -2Re(\tilde{\epsilon}_B) = O(10^{-2})\,. \tag{123}$$

Since B_L and B_H have almost identical lifetimes, it is impossible to produce selectively beams of B_L- and B_H-particles. The time evolution of an initially pure B^0-state is

$$|B^0(t)> = e^{-im_B t}e^{-\frac{1}{2}\Gamma_B t}(\cos(\frac{1}{2}\Delta m_B t)|B^0> + \frac{iq}{p}\sin(\frac{1}{2}\Delta m_B t)|\tilde{B}^0>)\,, \tag{124}$$

$$|\tilde{B}^0(t)> = e^{-im_B t}e^{-\frac{1}{2}\Gamma_B t}(\cos(\frac{1}{2}\Delta m_B t)|\tilde{B}^0> + \frac{ip}{q}\sin(\frac{1}{2}\Delta m_B t)|B^0>)\,, \tag{125}$$

where $m_{H,L} = m_B \pm \frac{1}{2}\Delta m_B$ and $\Gamma_{H,L} \simeq \Gamma_B$. Defining the semileptonic asymmetry as

$$a_{SL}^B = \frac{\Gamma(\tilde{B}^0(t) \to l^+\bar{\nu}X) - \Gamma(B^0(t) \to l^-\nu X)}{\Gamma(\tilde{B}^0(t) \to l^+\bar{\nu}X) + \Gamma(B^0(t) \to l^-\nu X)}\,, \tag{126}$$

one can find that

$$a_{SL}^B = \frac{1 - |q/p|^4}{1 + |q/p|^4} \simeq 4Re(\tilde{\epsilon}_B) = O(10^{-2})\,. \tag{127}$$

At present we don't have experimental evidence for indirect CP-violation in the B-meson system.

Consider decays of neutral mesons into CP-eigenstates:

$$A =< f_{CP}|H|P^0 >, \;\; A^* =< f_{CP}|H|\tilde{P}^0 > \; . \tag{128}$$

The condition $\lambda = \frac{q}{p} \cdot \frac{\tilde{A}}{A} \neq 1$ implies CP-violation. The most theoretically favoured scenario is when $\lambda = e^{i\phi_\lambda}$. In that case λ is a pure phase and hadronic uncertainties are cancelled. Define the CP-asymmetry as

$$a_{f_{CP}} = \frac{\Gamma(B^0(t) \to f_{CP}) - \Gamma(\tilde{B}^0(t) \to f_{CP})}{\Gamma(B^0(t) \to f_{CP}) + \Gamma(\tilde{B}^0(t) \to f_{CP})} . \tag{129}$$

Taking into account that $|\frac{q}{p}|_B \simeq 1$ we find that

$$a_{f_{CP}} \simeq \frac{(1 - |\lambda|^2)\cos(\Delta m_B t) - 2Im\lambda \sin(\Delta m_B t)}{1 + |\lambda|^2} . \tag{130}$$

Decays of neutral B-mesons into CP-eigenstates provide for model-independent determination of CP-violating phase. In the B-meson system we have

$$(\frac{q}{p})_B \simeq -\frac{M_{12}^*}{|M_{12}|} = \frac{(V_{tb}^* V_{td})^2}{|V_{tb}^* V_{td}|^2} = \frac{V_{tb}^* V_{td}}{V_{tb} V_{td}^*} = e^{-2i\beta} . \tag{131}$$

To eliminate hadronic uncertainties it is necessary to choose decay modes dominated by a single diagram. Examples of such decays are $\tilde{B} \to \pi\pi$, $\tilde{B} \to D\tilde{D}$, $B_s \to \phi K_S$, $\tilde{B} \to \rho K_S$, $B_S \to \psi K_S$, $\tilde{B} \to \phi K_S$, $\tilde{B} \to K_S K_S$, $B_s \to \eta' \eta'$, $B_s \to \phi K_S$, and $B_s \to \psi\phi$.

Tree-Dominated Decays: $\tilde{B} \to \pi\pi$. The decay $\tilde{B} \to \pi\pi$ proceeds through the quark decay $b \to u\bar{u}d$, for which both the tree and the penguin diagrams have CKM parameters of order λ^3. So the tree diagram is dominant and

$$\lambda_{\pi\pi} = \frac{q}{p} \cdot \frac{\tilde{A}}{A} \simeq \frac{V_{tb}^* V_{td}}{V_{tb} V_{td}^*} \cdot \frac{V_{ub} V_{ud}^*}{V_{ub}^* V_{ud}} = e^{-2i\beta} e^{-2i\gamma} = e^{2i\alpha} , \tag{132}$$

$$Im(\lambda_{\pi\pi}) \simeq \sin(2\alpha) . \tag{133}$$

Hadronic uncertainties arise from the small admixture of penguin contributions and they are expected to be of the order of 10 per cent.

Tree-Forbidden Decays: $\tilde{B} \to \phi K_S$. The decay $\tilde{B} \to \phi K_S$ proceeds through the quark transition $b \to s\bar{s}s$, i.e., it is forbidden at tree level and only penguin diagram contributes. A new ingredient here is the presence of $K - \tilde{K}$ mixing which adds a factor

$$(\frac{q}{p})_K \simeq \frac{V_{cs} V_{cd}^*}{V_{cs}^* V_{cd}} \tag{134}$$

in the definition of λ. One can find that

$$\lambda_{\phi K_S} = (\frac{q}{p})_B \cdot (\frac{q}{p})_K \cdot \frac{\bar{A}}{A} \simeq \frac{V_{tb}^* V_{td}}{V_{tb} V_{td}^*} \cdot \frac{V_{cs} V_{cd}^*}{V_{cs}^* V_{cd}} \cdot \frac{V_{tb} V_{ts}^*}{V_{tb}^* V_{ts}} = e^{-2i\beta}\,, \tag{135}$$

$$Im(\lambda_{\phi K_S}) \simeq -\sin(2\beta)\,. \tag{136}$$

Decays with a Single Weak Phase: $\tilde{B} \to \psi K_S$. The decay $\tilde{B} \to \psi K_S$ is based on the quark transition $b \to c\bar{c}s$, for which the tree diagram is dominant. One can find that

$$\lambda_{\psi K_S} = -(\frac{q}{p})_B \cdot (\frac{q}{p})_K \cdot \frac{\bar{A}}{A} \simeq -e^{-2i\beta}\,, \tag{137}$$

$$Im(\lambda_{\psi K_S}) \simeq \sin(2\beta)\,. \tag{138}$$

The hadronic uncertainties for this decay are of the order of 10^{-3}.

Note that the angle β' appearing in the CP-asymmetries for B_s-meson decay is the analogue of the angle β in the unitarity triangle defined by the relation

$$V_{us} V_{ub}^* + V_{cs} V_{cb}^* + V_{ts} V_{tb}^* = 0\,. \tag{139}$$

Experimentally $|\sin(2\beta')| \leq 0.06$.

3.2.5. B-Physics at CMS

Three experiments are foreseen for the B-physics investigation at LHC. ATLAS and CMS are two general purpose experiments designed to look for Higgs boson and supersymmetric particles. LHC-B [26] is a dedicated experiment for the CP-violation study. Since ATLAS and CMS are designed to look for particles produced in a very hard collision, detectors cover the central region. For the initial phase of the LHC operation where the luminosity is around $10^{33}\mathrm{cm}^{-2}\mathrm{s}^{-1}$, they intend to do physics with B-mesons. The b-quark events are triggered by the high transverse momentum (p_t) lepton trigger by reducing the threshold value.

LHC-B chose the forward geometry due to the following reasons [27]:

1. The b-quark production is peaked in the forward direction and in the forward region both b and $\bar{b}$ go to the same direction. Therefore, a single-arm spectrometer with a modest angular coverage of up to ~ 400 mrad can detect 10 to 20 per cent of $b\bar{b}$-events where decay products of both the b-hadrons are in detector acceptance. This reduces the cost of the detector.

2. B-hadrons produced in the forward direction are faster than those in the central region. Their average momentum is about 80 GeV, corresponding to a mean decay length of ~ 7 mm. Therefore, a good decay time resolution can be obtained for reconstructed B-mesons.

3. In the forward region, momenta are mainly carried by the longitudinal components. Therefore, the threshold value for p_t-trigger can be set low for electrons, muons and hadrons around 1.5 GeV. This makes p_t-trigger more efficient than in the central region.

4. Detector can be built in an open geometry which allows easy installation and maintenance.

5. LHC-B is only the detector capable of separating kaons from pions in all necessary phase space.

Here we briefly describe the B-physics potential of CMS. ATLAS B-physics potential is similar to CMS one. As it has been mentioned before the main CP-violation prediction for B-systems is the inequality $\Gamma(B^0 \to f) \neq \Gamma(\bar{B}^0 \to \bar{f})$. The decay rate asymmetry

$$A = \frac{\Gamma(B^0 \to f) - \Gamma(\bar{B}^0 \to \bar{f})}{\Gamma(B^0 \to f) + \Gamma(\bar{B}^0 \to \bar{f})} \sim \sin(2\Phi) \tag{140}$$

depends only on CP-violating angles of triangle $\alpha, \gamma, \beta = \Phi$. At LHC the cross section $pp \to b\bar{b} + ...$ is expected to be in the range $0.08 - 0.6$ mb. The most promising channels for the search for the CP-violation are:

$$B_d^0 \to (\psi \to \mu^+\mu^-) + (K_s^0 \to \pi^+\pi^-) \text{ and } B_d^0 \to \pi^+\pi^-.$$

The decay $B_d^0 \to \psi K_S^0$ with $\psi \to \mu^+\mu^-$ and $K_S^0 \to \pi^+\pi^-$ is the most appropriate channel to measure the angle β. To tag the B_d^0, the associated b-hadron is required to decay into muon + X. The time integrated asymmetry A is:

$$A = \frac{N^+ - N^-}{N^+ + N^-} = D \cdot \frac{x_d}{1 + x_d^2} \cdot \sin(2\beta)\,, \tag{141}$$

where N^+ and N^- are the number of events with positively and negatively charged tagging muons, D is the dilution factor and $\frac{x_d}{1+x_d^2}$ is the time-integration factor. The expected number of events for an integrated luminosity L is:

$$N = 2 \times L \times \sigma_{b\bar{b}} \times P(\bar{b} \to B_d^0) \times Br(B_d^0 \to \psi K_S^0) \times \\ \times Br(\psi \to \mu^+\mu^-) \times Br(K_S^0 \to \pi^+\pi^-) \times Br(b \to \mu) \times A_{trig} \times \epsilon\,, \tag{142}$$

where A_{trig} is the trigger acceptance and ϵ is the efficiency of the selection cuts. Typical values of the branching ratios are: $P(\bar{b} \to B_d^0) = 0.4$; $Br(B_d^0 \to \psi K_S^0) = 3.3 \times 10^{-4}$; $Br(\psi \to \mu^+\mu^-) = 0.0597$; $Br(K_S^0 \to \pi^+\pi^-) = 0.6861$; $Br(b \to \mu) = 0.105$. Before trigger-acceptance and data-selection cuts, the number of produced signal events is 5.6×10^6 for 10^4 pb^{-1}. The measured asymmetry A is affected by dilution factors $D \simeq 0.47$. The signal to background ratio is estimated to be $S/b \approx 10 : 1$ and the mixing angle $\sin(2\beta)$ accuracy determination is ≈ 0.05 for $L_t = 10^4$ pb^{-1}.

The $B_d^0 \to \pi^+\pi^-$ decay is a good channel to determine the angle α of the unitarity triangle. For $L_t = 10^4$ pb^{-1} the sensitivity to the triangle angle α determination is estimated to be:

$$\delta(\sin(2\alpha)) = 0.057 \pm 0.018 \ .$$

CP-violation in B_d^0 and $\tilde{B}_d^0$ decays gives rise to different decay rates with a time dependence. The asymmetry can be measured as a function of proper time t/τ in units of the B_d^0 lifetime τ:

$$A(t/\tau) = \frac{N^- - N^+}{N^- + N^+} = D \cdot \eta_{CP} \cdot \sin(2\varphi_i) \cdot \sin(x_d t/\tau)\,, \qquad (143)$$

where N^+ and N^- are the numbers of events with positively and negatively charged tagging muons, D is the dilution factor, η_{CP} is the CP-parity of the final state f and φ_i is the angle of the unitarity triangle. It is possible to measure the secondary vertex in the transverse plane to determine time-dependent asymmetry and hence to determine the CP-violating angles α and β [1]. The accuracy in the determination of the angles α and β is similar to the accuracy for the case of the time integrated asymmetry considered previously.

Very important task of B-physics at LHC is the observation of $B_s^0 - \bar{B}_s^0$ oscillations but it could be very difficult if x_s is large. The current limits on the value of x_s are $5.6 \leq x_s \leq 33.2$ [28]. The possibility to discover $B_s^0 - \bar{B}_s^0$ oscillations at LHC has been studied in Refs. 29.

Other interesting task is the search for $B_s^0 \to \mu^+\mu^-$ rare decay. This decay is forbidden at tree level. In standard model, the branching ratio of this decay is expected to be $\approx 2 \times 10^{-9}$ [30]. It appears that at CMS the upper limit on this branching ratio can be set 1.4×10^{-9} at a 90 per cent C.L. for $L_t = 3 \times 10^4$ pb^{-1} [1].

3.2.6. Heavy Ion Physics

Quantum chromodynamics has already proved itself to be a reliable theory when dealing with quark and gluon interactions at short distances. The QCD vacuum shows properties which are similar to those of a superconductor. It has a critical temperature beyond which it becomes transparent to colour. This temperature is found to be of the order of 150–200 MeV [31]. Consider a system consisting of a set of hadrons in the vacuum and compress it. The hadrons are initially too far to overlap. As the density increases they start overlapping among themselves. We thus go from a dilute to a very dense hadron gas. With increasing compression the hadrons merge among one another. The small vacuum bubbles separately associated with each individual hadron should eventually fuse into one big bubble within which quarks would freely move over distances much larger than those offered by the hadrons in which they were first confined. Since in

high energy collisions new particles are created out of the collision energy, we reach the same conclusions if the initial dilute hadron gas is heated instead of being merely compressed. In heavy ion collisions we have a complicated mixture of compression and heating. Computer calculations support the naive picture according to which at low temperature we have hadron gas and at high temperature we have quark-gluon plasma [31]. Naively we can expect the following picture in heavy ion collisions at high energies [31]:

1. An initial phase during which many collisions occur at the parton level. A large number of energetic partons are formed. The system is still far from any equilibrium. A large amount of entropy is released.

2. A thermalized phase, obtained through the scattering of the many partons. The temperature is very high. The system is a quark-gluon plasma, at least in some localized regions.

3. A mixed phase, obtained as the plasma cools with parts of it hadronizing as the temperature goes through its critical value.

4. A thermalized, dense, hadron gas from which hadrons eventually escape as their mean free path exceeds the size of the system. This is what is referred to as freeze out.

However all the processes occur in a very short time. When we look at the dominantly produced hadrons we merely integrate over the whole evolution. So any evidence for a quark-gluon plasma is averaged out the past history. In other words after the transition from quark-gluon plasma to hadron phase the system can "forget" about previous phase. The most striking signal associated with quark-gluon plasma is the suppression of the charmonium and upsilonium formation [32].

The physical picture leading to the ψ suppression due to quark deconfinement in nuclear collisions is quite simple. Within a deconfining medium like QGP (quark-gluon plasma), quarks cannot bind to form hadrons. Heavy charm quark-antiquark pairs which form ψ are produced by hard, prethermal interactions at a very early stage of the collision. In a deconfining medium c and $\bar{c}$ just fly apart. Moreover, within the equilibrated QGP the production of additional thermal c quarks is strongly suppressed by a factor of $\exp(-m_c/T_c) \simeq 0.6 \times 10^{-3}$ with a mass of charm quark $m_c = 1.5$ GeV and $T_c = 0.2$ GeV. Consequently ψ production will be suppressed in the presence of QGP. In atomic physics, the screened binding potential between two charges is given by $V = V_o \exp(-r/r_D)$, where r_D is the Debye radius. When $r_D \approx r_B$ the valence electrons are liberated owing to charge screening and the insulator changes into a conductor. Similarly, in QCD the potential between two coloured quarks is given by $V = V_0 \exp(-r/r_D)$ because of colour screening, and if the density of colour charges is sufficient to make $r_D \leq r_H$ (hadron radius), colour insulators of hadrons change into colour-conducting phase, i.e., QGP. It means that the long range confining phase of the potential gets screened, i.e., we have quark deconfinement. We have to

know the ψ radius and the screening radius r_D at a given temperature. Only for $r_D \leq r_\psi$ we can expect ψ suppression. It has been found [31] that $r_D = r_H$ occurs near the transition temperature T_c for ψ' and $T/T_c \geq 1.3$ for ψ. Recent data of NA50 [33] support this picture. It should be noted however that ψ suppression can also be explained either on the basis of absorption processes in a dense hadron gas or on the basis of conventional nuclear effects [34]. For LHC energies with the center of mass energy around 6 TeV per nucleon and with the energy density $\epsilon \approx 9$ GeV/fm^3 all heavy quark bound states except for $\Upsilon(1S)$ will be suppressed by colour screening.

The main goal of LHC heavy ion program is the search for quark-gluon plasma. There will be special detector ALICE [35] dedicated for the heavy ion investigation at LHC. Here we briefly describe the "heavy ion potential" of CMS [1]. The most promising signature here is the measurement of the production rates of the bottonium states for different nuclei and different kinematics. The most interesting signature is the measurement of the cross section of Υ state as a function of p_T^Υ since no suppression due to Debye colour screening is expected [31, 32]. As it has been mentioned before the typical prediction of the existence of quark-gluon plasma in this case is the suppression of $\Upsilon(2S)$ and $\Upsilon(3S)$ relative to $\Upsilon(1S)$ yield. Simulation studies were performed for ^{16}O, ^{40}Ca, ^{97}Nb and ^{208}Pb ion collisions. The ψ and Υ resonances were generated using p_t and y distributions extrapolated from experimental results obtained at lower $\sqrt{s}$. The total acceptance for $\Upsilon \to \mu\mu$ has been found ≈ 0.33, and for ψ it is around 0.06. If we restrict ourselves to the barrel region, where muons with $p_t \geq 4$ GeV can be detected, the acceptance for Υ decreases to 0.05 and for ψ it vanishes. It has been found that the mass resolution for Υ is around 40 MeV. The cross sections for Υ production in $A - A$ collisions were obtained multiplying the cross sections for pp reaction at the same c.m.s. energy by a factor of $A^{2\alpha}$ with $\alpha = 0.95$. The main dimuon background is due to uncorrelated muon pairs from π- and K-decays. The signal-to-background ratios have been calculated in the mass band $M(\Upsilon) \pm 50$ MeV, for central collisions of Pb, Ca, Nb and O beams. The results depend rather strongly on the value of $\sigma(pp \to \Upsilon)$ and on the charged particle multiplicity $dn^\pm/dy$ per unit rapidity in the central collision. The main conclusion from these studies is that CMS will be able to detect reliably Υ, Υ' and Υ'' resonances.

Other interesting prediction testable at CMS is the jet quenching in quark gluon plasma. As jets are produced early in a collision, they propagate in the plasma, and interact strongly before they escape. Hence, they carry information about deconfined hadronic matter. The problems of jet finding at CMS with the large transverse energy (E_t) flow in central collisions were studied, to determine the possibilities of observing jet quenching using CMS [36]. The high E_t-jet production cross section in $Pb - Pb$ collisions was estimated in the rapidity

region $|y| \leq 1.5$, using the jet cross section for pp-interactions, as evaluated by PYTHIA, and an $A^{2\alpha}$ dependence for the $A-A$ colllisions. The effect of energy losses in dense nuclear matter changing the high E_t-jet production cross section was not taken into account. A central event with two high E_t-jets from a proton-proton collision was superimposed on the ion collision. The main conclusion from these studies is that jets may be reliably reconstructed in the CMS detector for $Pb-Pb$ central collisions with $E_t \geq 100$ GeV [36].

3.3. Supersymmetry Search within MSSM

3.3.1. MSSM Model

Supersymmetry is a new type of symmetry that relates properties of bosons to those of fermions [37]. It is the largest symmetry of the S-matrix. Locally supersymmetric theories necessarily incorporate gravity [38]. SUSY is also an essential ingredient of superstring theories [39]. The recent interest in supersymmetry is due to the observation that measurements of the gauge coupling constants at LEP1 are in favour of the Grand Unification in a supersymmetric theory with superpartners of ordinary particles which are lighter than $O(1)$ TeV. Besides supersymmetric electroweak models offer the simplest solution of the gauge hierarchy problem [37]. In real life supersymmetry has to be broken and to solve the gauge hierarchy problem the masses of superparticles have to be lighter than $O(1)$ TeV. Supergravity gives natural explanation of the supersymmetry breaking [38], namely, an account of the supergravity breaking in hidden sector leads to soft supersymmetry breaking in observable sector. The simplest supersymmetric generalization of the standard model is the Minimal Supersymmetric Standard Model (MSSM). It is supersymmetric theory based on standard $SU_c(3) \otimes SU_L(2) \otimes U(1)$ gauge group with electroweak symmetry spontaneously broken via vacuum expectation values of two different Higgs doublets. The MSSM consists of taking the standard model and adding the corresponding supersymmetric partners. It should be stressed that in addition the MSSM contains two hypercharges $Y = \pm 1$ Higgs doublets, which is the minimal structure for the Higgs sector of an anomaly-free supersymmetric extension of the Standard Model. The supersymmetric electroweak models also require at least two Higgs doublets to generate masses for both "up"-type and "down"-type fermions. The renormalizable superpotential determines the Yukawa interactions of quarks and leptons and preserves global $B-L$. Here B is the baryon number and L is the lepton number. Note that the most general expression for the effective superpotential contains renormalizable terms violating $B-L$ that can lead to the problems with proton decay. To get rid of such dangerous terms in the superpotential, R-parity conservation of the theory is postulated. Here $R = (-1)^{3(B-L)+2S}$ for a particle of spin S. This formula means that all ordinary standard model particles have

$R = 1$, whereas the corresponding supersymmetric partners have $R = -1$. The R-parity conservation has a crusial impact on supersymmetric phenomenology. An important consequence of R-parity conservation is that the lightest supersymmetric particle (LSP) is stable. The cosmological constraints imply that LSP is weakly-interacting electrically neutral and colourless particle. Other important consequence of R-parity conservation is that at supercolliders superparticles have to be produced in pairs, therefore at least two LSP have eventually be produced at the end of the decays of heavy unstable supersymmetric particles. Being weakly interacting particle LSP escapes detector registration, therefore the classic signature for R-parity conserving supersymmetric theories is the transverse missing energy due to the LSP escape. Note that at present there are no deep theoretical arguments in favour of R-parity conservation. There are models with R-parity violation [40]. Models with R-parity violation break $B - L$ number and are strongly constrained by existing experimental data. In such models LSP is unstable, supersymmetric particles can be singly produced and in general the signature related with the transverse missing energy is lost.

The superpotential of MSSM has the form

$$W = h^u_{ij} U^c_i Q_j H_2 + h^d_{ij} D^c_i Q_j H_1 + h^l_{ij} E^c_i L_j H_1 - \mu H_1 H_2 \,, \qquad (144)$$

where i, j are summed over 1,2,3 and Q_j, U^c_a , D^c_b denote $SU(2)$-doublet and $SU(2)$-singlet quark superfields, L^i, E^c_i are the $SU(2)$-doublet and $SU(2)$-singlet lepton superfields and H_1, H_2 denote the two Higgs superdoublets, h^u_{ij}, h^d_{ij}, h^l_{ij} are the Yukawa coupling constants. In MSSM, supersymmetry is softly broken at some high scale M by generic soft terms

$$\begin{aligned} -L_{soft} = {} & m_0 (A^u_{ij} U^c_i Q_j H_2 + A^d_{ij} D^c_i G_j H_1 + \qquad (145) \\ & A^l_{ij} E^c_i L_j H_1 + h.c.) + (m^2_q)_{ij} Q^+_i Q_j + (m^2_u)_{ij} (U^c_i)^+ U^c_j + \\ & (m^2_d)_{ij} (D^c_i)^+ D^c_j + (m^2_l)_{ij} (L^c_i)^+ L^c_j + (m^2_e)_{ij} (E^c_i)^+ \\ & E^c_j + m^2_1 H_1 H^+_1 + m^2_2 H_2 H^+_2 + (B m_0{}^2 H_1 H_2 + h.c.) + \frac{1}{2} m_a (\lambda_a \lambda_a) \,. \end{aligned}$$

In most analysis the mass terms are supposed to be diagonal at $M_{\rm GUT} \approx 2 \cdot 10^{16}$ GeV scale and gaugino and trilinear mass terms are supposed to be universal at M_{GUT} scale, namely at GUT scale:

$$\begin{aligned} A^u_{ij}(M_{\rm GUT}) &= A h^u_{ij}(M_{\rm GUT}), \qquad (146) \\ A^d_{ij}(M_{\rm GUT}) &= A h^d_{ij}(M_{\rm GUT}), \\ A^l_{ij}(M_{\rm GUT}) &= A h^l_{ij}(M_{\rm GUT}), \end{aligned}$$

$$(m^2_q)_{ij}(M_{\rm GUT}) = (m^2_u)_{ij}(M_{\rm GUT}) = (m^2_d)_{ij}(M_{\rm GUT}) = \qquad (147)$$

$$(m_l^2)_{ij}(M_{\rm GUT}) = (m_e^2)_{ij}(M_{\rm GUT}) = \delta_{ij} m_1^2(M_{\rm GUT}) = \delta_{ij} m_2^2(M_{\rm GUT}) = \delta_{ij} m_0^2\,,$$

$$m_1(M_{\rm GUT}) = m_2(M_{\rm GUT}) = m_3(M_{\rm GUT}) = m_{1/2}\,. \tag{148}$$

Note that it is more appropriate to impose boundary conditions not at GUT scale but at Planck scale $M_{PL} = 2.4 \cdot 10^{18}$ GeV. An account of the renormalization effects between PLANCK scale and GUT scale can drastically change the features of the spectrum. For instance, if we assume that the physics between Planck scale and GUT scale is described by SUSY SU(5) model then an account of the evolution between PLANCK and GUT scales [41,42] changes qualitatively the spectrum of sleptons for $m_0 \ll m_{1/2}$ [42]. So in MSSM we have unknown soft supersymmetry breaking parameters m_0, $m_{1/2}$, A, B plus we have unknown parameter μ in the superpotential. The renormalization group equations for soft SUSY breaking parameters in neglection of all Yukawa coupling constants except top-quark Yukawa in one-loop approximation read [43]

$$\frac{d\tilde{m}_L^2}{dt} = (3\tilde{\alpha}_2 M_2^2 + \frac{3}{5}\tilde{\alpha}_1 M_1^2)\,, \tag{149}$$

$$\frac{d\tilde{m}_E^2}{dt} = (\frac{12}{5}\tilde{\alpha}_1 M_1^2)\,, \tag{150}$$

$$\frac{d\tilde{m}_Q^2}{dt} = (\frac{16}{3}\tilde{\alpha}_3 M_3^2 + 3\tilde{\alpha}_2 M_2^2 + \frac{1}{15}\tilde{\alpha}_1 M_1^2) - \delta_{i3} Y_t(\tilde{m}_Q^2 + \tilde{m}_U^2 + m_2^2 + A_t^2 m_0^2 - \mu^2)\,, \tag{151}$$

$$\frac{d\tilde{m}_U^2}{dt} = (\frac{16}{3}\tilde{\alpha}_3 M_3^2 + \frac{16}{15}\tilde{\alpha}_1 M_1^2) - \delta_{i3} 2Y_t(\tilde{m}_Q^2 + \tilde{m}_U^2 + m_2^2 + A_t^2 m_0^2 - \mu^2)\,, \tag{152}$$

$$\frac{d\tilde{m}_D^2}{dt} = (\frac{16}{3}\tilde{\alpha}_3 M_3^2 + \frac{4}{15}\tilde{\alpha}_1 M_1^2)\,, \tag{153}$$

$$\frac{d\mu^2}{dt} = 3(\tilde{\alpha}_2 + \frac{1}{5}\tilde{\alpha}_1 - Y_t)\mu^2\,, \tag{154}$$

$$\frac{dm_1^2}{dt} = 3(\tilde{\alpha}_2 M_2^2 + \frac{1}{5}\tilde{\alpha}_1 M_1^2) + 3(\tilde{\alpha}_2 + \frac{1}{5}\tilde{\alpha}_1 - Y_t)\mu^2\,, \tag{155}$$

$$\frac{dm_2^2}{dt} = 3(\tilde{\alpha}_2 M_2^2 + \frac{1}{5}\tilde{\alpha}_1 M_1^2) + 3(\tilde{\alpha}_2 + \frac{1}{5}\tilde{\alpha}_1)\mu^2 - 3Y_t(\tilde{m}_Q^2 + \tilde{m}_U^2 + m_2^2 + A_t^2 m_0^2)\,, \tag{156}$$

$$\frac{dA_t}{dt} = -(\frac{16}{3}\tilde{\alpha}_3 \frac{M_3}{m_0} + 3\tilde{\alpha}_2 \frac{M_2}{m_0} + \frac{13}{15}\tilde{\alpha}_1 \frac{M_1}{m_0})) - 6Y_t A_t\,, \tag{157}$$

$$\frac{dB}{dt} = -3(\tilde{\alpha}_2 \frac{M_2}{m_0} + \frac{1}{5}\tilde{\alpha}_1 \frac{M_1}{m_0}) - 3Y_t A_t\,, \tag{158}$$

$$\frac{dM_i}{dt} = -b_i\tilde{\alpha}_i M_i\,, \tag{159}$$

$$b_1 = \frac{33}{5},\ b_2 = 1,\ b_3 = -3\,. \tag{160}$$

Here $\tilde{m}_U$, $\tilde{m}_D$, $\tilde{m}_E$ refer to the masses of the superpartner of the quark and lepton singlets, while $\tilde{m}_Q$ and $\tilde{m}_L$ refer to the masses of the isodoublet partners; m_1, m_2, m_3 and μ are the mass partners of the Higgs potential, A and B are the couplings of the L_{soft} as defined before; M_i are the gaugino masses before mixing. The renormalization group equation for the top Yukawa coupling constant has the form

$$\frac{dY_t}{dt} = Y_t(\frac{16}{3}\tilde{\alpha}_3 + 3\tilde{\alpha}_2 + \frac{13}{15}\tilde{\alpha}_1) - 6Y_t^2\,, \tag{161}$$

while the RG equations for the gauge couplings are

$$\frac{d\tilde{\alpha}_i}{dt} = -b_i\tilde{\alpha}_i^2\,. \tag{162}$$

Here

$$\tilde{\alpha}_i = \frac{\alpha_i}{4\pi},\ Y_t = \frac{h_t^2}{16\pi^2},\ t = \ln(\frac{M_{\rm GUT}^2}{Q^2})\,, \tag{163}$$

and the top Yukawa coupling h_t is related to the running top mass by the relation

$$m_t = h_t(m_t)\frac{v}{\sqrt{2}}\sin\beta\,. \tag{164}$$

The boundary conditions at $Q^2 = M_{\rm GUT}^2$ are

$$\tilde{m}_Q^2 = \tilde{m}_U^2 = \tilde{m}_D^2 = \tilde{m}_E^2 = \tilde{m}_L^2 = m_0^2\,, \tag{165}$$

$$\mu = \mu_0;\ m_1^2 = m_2^2 = \mu_0^2 + m_0^2;\ m_3^2 = B\mu_0 m_0\,, \tag{166}$$

$$M_i = m_{1/2},\ \tilde{\alpha}_i(0) = \tilde{\alpha}_{\rm GUT};\ i = 1,2,3\,. \tag{167}$$

For the gauginos of the $SU(2)\otimes U(1)$ gauge group one has to consider the mixings with the Higgsinos. The mass terms in the full Lagrangian are [44]

$$L_{Gaugino-Higgsino} = -\frac{1}{2}M_3\bar{\lambda}_3^a\lambda_3^a - \frac{1}{2}\bar{\chi}M^{(0)}\chi - (\bar{\psi}M^{(c)}\psi + h.c.)\,, \tag{168}$$

where λ_3^a are the 8 Majorana gluino fields, and

$$\chi = \begin{pmatrix} \tilde{B}^0 \\ \tilde{W}^3 \\ \tilde{H}_1^0 \\ \tilde{H}_2^0 \end{pmatrix}, \tag{169}$$

$$\psi = \begin{pmatrix} \tilde{W}^+ \\ \tilde{H}^+ \end{pmatrix}, \tag{170}$$

are the Majorano neutralino and Dirac chargino fields. The mass matrices are:

$$M^{(0)} = \begin{pmatrix} M_1 & 0 & -A & B \\ 0 & M_2 & C & -D \\ -A & C & 0 & -\mu \\ B & -D & -\mu & 0 \end{pmatrix}, \tag{171}$$

$$M^{(c)} = \begin{pmatrix} M_2 & \sqrt{2}M_W \sin\beta \\ \sqrt{2}M_W \cos\beta & \mu \end{pmatrix}, \tag{172}$$

where:

$$A = M_Z \cos\beta \sin\theta_W, \; B = M_Z \sin\beta \sin\theta_W, \tag{173}$$

$$C = M_Z \cos\beta \cos\theta_W, \; D = M_Z \sin\beta \cos\theta_W. \tag{174}$$

After the solution of the corresponding renormalization group equations for $\alpha_{\rm GUT} = \frac{1}{24.3}$, $M_{\rm GUT} = 2.0 \cdot 10^{16}$ GeV, $\sin^2\theta_W = 0.2324$ and $A_t(0) = 0$ one finds the numerical formulae for squark and slepton square masses [45]

$$\tilde{m}^2_{E_L}(t = 66) = m_0^2 + 0.52m^2_{1/2} - 0.27\cos 2\beta M_Z^2, \tag{175}$$

$$\tilde{m}^2_{\nu_L}(t = 66) = m_0^2 + 0.52m^2_{1/2} + 0.5\cos 2\beta M_Z^2, \tag{176}$$

$$\tilde{m}^2_{E_R}(t = 66) = m_0^2 + 0.15m^2_{1/2} - 0.23\cos 2\beta M_Z^2, \tag{177}$$

$$\tilde{m}^2_{U_L}(t = 66) = m_0^2 + 6.5m^2_{1/2} + 0.35\cos 2\beta M_Z^2, \tag{178}$$

$$\tilde{m}^2_{D_L}(t = 66) = m_0^2 + 6.5m^2_{1/2} - 0.42\cos 2\beta M_Z^2, \tag{179}$$

$$\tilde{m}^2_{U_R}(t = 66) = m_0^2 + 6.1m^2_{1/2} + 0.15\cos 2\beta M_Z^2, \tag{180}$$

$$\tilde{m}^2_{D_R}(t = 66) = m_0^2 + 6.0m^2_{1/2} - 0.07\cos 2\beta M_Z^2, \tag{181}$$

$$\tilde{m}^2_{b_R}(t = 66) = \tilde{m}^2_{D_R}, \tag{182}$$

$$\tilde{m}^2_{b_L}(t = 66) = \tilde{m}^2_{D_L} - 0.49m_0^2 - 1.21m^2_{1/2}, \tag{183}$$

$$\tilde{m}^2_{t_R}(t = 66) = \tilde{m}^2_{t_R}(t = 66) = \tilde{m}^2_{U_R}(t = 66) + m_t^2 - 0.99m_0^2 - 2.42m^2_{1/2}, \tag{184}$$

$$\tilde{m}^2_{t_L}(t = 66) = \tilde{m}^2_{U_L}(t = 66) + m_t^2 - 0.49m_0^2 - 1.21m^2_{1/2}. \tag{185}$$

After mixing the mass eigenstates of the stop matrix are:

$$\tilde{m}^2_{t_{1,2}}(t = 66) \approx \frac{1}{2}[0.5m_0^2 + 9.1m^2_{1/2} + 2m_t^2 + 0.5\cos 2\beta M_Z^2] \tag{186}$$

$$\mp\frac{1}{2}[(1.5m^2_{1/2} + 0.5m_0^2 + 0.2\cos(2\beta)M_Z^2)^2 + 4m_t^2(A_t m_o - \mu/\tan\beta)^2]^{1/2}.$$

The gauginos and Higgsinos have similar quantum numbers which causes a mixing between the weak interaction eigenstates and the mass eigenstates. The two chargino eigenstates $\chi^{\pm}_{1,2}$ are:

$$M^2_{1,2} = \frac{1}{2}[M_2^2 + \mu^2 + 2M_W^2] \mp \frac{1}{2}[(M_2^2 - \mu^2)^2 + 4M_W^4 \cos^2 2\beta$$
$$+4M_W^2(M_2^2 + \mu^2 + 2M_2\mu \sin 2\beta)]^{1/2}\,, \qquad (187)$$

where at GUT scale the masses of the gaugino fields of the $SU(3)$, $SU_L(2)$ and $U(1)$ groups are equal to $m_{1/2}$. The eigenvalues of the 4×4 neutralino mass matrix can be solved by a numerical diagonalization. If the parameter μ is much larger than M_1 and M_2, the mass eigenstates become

$$\chi^0_i = [\tilde{B}, \tilde{W}_3, \frac{1}{\sqrt{2}}(\tilde{H}_1 - \tilde{H}_2), \frac{1}{\sqrt{2}}(\tilde{H}_1 + \tilde{H}_2)] \qquad (188)$$

with eigenvalues $|M_1|$, $|M_2|$, $|\mu|$ and $|\mu|$, respectively (the bino and neutral wino do not mix with each other nor with the Higgsino eigenstates).

The tree-level Higgs potential in MSSM has the form

$$V_0(H_1, H_2) = m_1^2|H_1|^2 + m_2^2|H_2|^2 - m_3^2(H_1H_2 + h.c) +$$
$$\frac{g_2^2 + \tilde{g}_1^2}{8}(|H_1|^2 - |H_2|^2)^2 + \frac{g_2^2}{2}|H_1^+H_2|^2\,, \qquad (189)$$

where $\tilde{g}_1^2 = \frac{3}{5}g_1^2$.

The minimization of the effective potential $V_0(H_1, H_2)$ leads to the equations:

$$v^2 = \frac{8(m_1^2 - m_2^2 \tan^2\beta)}{(g_2^2 + \tilde{g}_1^2)(\tan^2\beta - 1)}\,, \qquad (190)$$

$$\sin 2\beta = \frac{2m_3^2}{m_1^2 + m_2^2}\,. \qquad (191)$$

After the diagonalization of the corresponding mass matrices CP-odd neutral Higgs boson $A(x)$ acquires a mass $m_A^2 = m_1^2 + m_2^2$, charged Higgs boson $H^+(x)$ acquires a mass $m_{H^+}^2 = m_A^2 + M_W^2$ and CP-even Higgs bosons $H(x)$ and $h(x)$ have masses

$$m^2_{H,h} = \frac{1}{2}[m_A^2 + M_Z^2 \pm \sqrt{(m_A^2 + M_Z^2)^2 - 4m_A^2M_Z^2\cos^2 2\beta}]\,, \qquad (192)$$

where $< H_1 >= v_1 = \frac{v\cos\beta}{\sqrt{2}}$, $< H_2 >= v_2 = \frac{v\sin\beta}{\sqrt{2}}$, $\tan\beta = \frac{v_2}{v_1}$. At tree-level we have the following mass relations:

$$m_h^2 + m_H^2 = m_A^2 + M_Z^2\,, \qquad (193)$$

$$m_h \leq m_A \leq m_H \,, \tag{194}$$

$$m_h \leq M_Z |\cos 2\beta| \leq M_Z \,. \tag{195}$$

Therefore at tree-level the lightest Higgs boson is lighter than the Z-boson. However the radiative corrections due to big top quark Yukawa coupling constant increase the mass of the lightest Higgs boson in MSSM [46]. The upper limit on the Higgs boson mass in MSSM depends on the value of the top quark mass and on the value of stop quark masses. For instance, for $m_t = 175$ GeV and stop quark masses lighter than 1 TeV, the Higgs boson mass, as it follows from the Table, has to be lighter than 117 GeV. From the vacuum stability bound ($k = 0$ in the Table) we find that if standard model is valid for energies up to 10^6 GeV, then the mass of the Higgs boson has to be heavier than 121 GeV for $m_t = 175$ GeV. Therefore for $m_t = 175$ GeV we find that the Higgs boson mass predictions for SM and MSSM lie in different mass intervals (in MSSM Higgs boson is relatively light, whereas in SM it is relatively heavy). So the exact knowledge of the Higgs boson mass allows one to distinguish between SM and MSSM [47]. For instance, the Higgs boson discovery at LEP2 will be very powerful evidence in favour of the low energy broken supersymmetry. After the solution of the corresponding equations for the determination of nontrivial electroweak potential the number of unknown parameters is decreased by 2. At present more or less standard choice of free parameters in MSSM includes m_0, $m_{1/2}$, $\tan\beta$, A and sign(μ).

Superparticle Cross Sections. At LHC, sparticles can be produced via the following tree-level reactions [48]:

i. $gg, qq, qg \to \tilde{g}\tilde{g},\ \tilde{g}\tilde{q},\ \tilde{q}\tilde{q}$,

ii. $qq, gq \to \tilde{g}\chi_i^0,\ \tilde{g}\chi_i^{\pm},\ \tilde{q}\chi_i^0,\ \tilde{q}\chi_i^{\pm}$,

iii. $qq \to \chi_i^{\pm}\chi_j^{\mp},\ \chi_i^{\pm}\chi_j^0,\ \chi_i^0\chi_j^0$,

iiii. $qq \to \tilde{l}\tilde{\nu},\ \tilde{l}\tilde{l},\ \tilde{\nu}\tilde{\nu}$,

The Higgs bosons of the MSSM can be produced via direct s-channel subprocess:

iiiii. $qq, gg \to h,\ H,\ A,\ H^{\pm}H^{\mp}$.

It is straightforward to calculate the elementary (tree-level) cross sections for the production of superparticles in collisions of quarks and gluons. Here, following E.Eichten et al. [4], we collect the main formulae for elementary cross sections.

The differential cross section of the production of two gauge fermions in quark-antiquark collisions is

$$\frac{d\sigma}{dt}(q\bar{q}^{'} \to gaugino1 + gaugino2) = \tag{196}$$

$$\frac{\pi}{s^2}[A_s\frac{(t-m_2^2)(t-m_1^2)+(u-m_1^2)(u-m_2^2)+2sm_1m_2}{(s-M_s^2)^2}+$$
$$A_t\frac{(t-m_1^2)(t-m_2^2)}{(t-M_t^2)^2}+$$
$$A_u\frac{(u-m_1^2)(u-m_2^2)}{(u-M_u^2)^2}+A_{st}\frac{(t-m_1^2)(t-m_2^2)+m_1m_2s}{(s-M_s^2)(t-M_t^2)}+$$
$$A_{tu}\frac{m_1m_2s}{(t-M_t^2)(u-M_u^2)}+A_{su}\frac{(u-m_1^2)(u-m_2^2)+m_1m_2s}{(s-M_s^2)(u-M_u^2)}],$$

where m_1 and m_2 are the masses of the produced gauginos, M_s, M_t and M_u are the masses of the particles exchanged in the s,t, and u channels, respectively. The coefficients A_x are given in paper of E.Eichten et al. [4]. For instance, for the case of the gluino pair production in quark-antiquark collisions the coefficients A_x are [4]:

$$A_t=\tfrac{4}{9}A_s,\ A_u=A_t,\ A_{st}=A_s,\ A_{su}=A_{st},\ A_{tu}=\tfrac{1}{9}A_s,\ A_s=\tfrac{8\alpha_s^2}{3}\delta_{qq'}\ .$$

The differential cross section for the production of gluino pairs in gluon-gluon collisions is

$$\frac{d\sigma}{dt}(gg\to\tilde{g}\tilde{g})= \tag{197}$$
$$\frac{9\pi\alpha_s^2}{4s^2}[\frac{2(t-m_{\tilde{g}}^2)(u-m_{\tilde{g}}^2)}{s^2}+[[\frac{(t-m_{\tilde{g}}^2)(u-m_{\tilde{g}}^2)-2m_{\tilde{g}}^2(t+m_{\tilde{g}}^2)}{(t-m_{\tilde{g}}^2)^2}+$$
$$\frac{(t-m_{\tilde{g}}^2)(u-m_{\tilde{g}}^2)+m_{\tilde{g}}^2(u-t)}{s(t-m_{\tilde{g}}^2)}]+(t\leftrightarrow u)]+$$
$$\frac{m_{\tilde{g}}^2(s-4m_{\tilde{g}}^2)}{(t-m_{\tilde{g}}^2)(u-m_{\tilde{g}}^2)}].$$

The total cross section has the form

$$\sigma(gg\to\tilde{g}\tilde{g})=\frac{3\pi\alpha_s^2}{4s}[3[1+\frac{4m_{\tilde{g}}^2}{s}-\frac{4m_{\tilde{g}}^4}{s^2}]\ln[\frac{s+L}{s-L}]-[4+\frac{17m_{\tilde{g}}^2}{s}]\frac{L}{s}], \tag{198}$$

where $L=[s^2-4m_{\tilde{g}}^2s]^{1/2}$.

The differential cross section for the reaction $q_iq_j\to\tilde{q}_i\tilde{q}_j$ for the case of equal masses of right-handed and left-handed squarks is

$$\frac{d\sigma}{dt}(q_iq_j\to\tilde{q}_i\tilde{q}_j)= \tag{199}$$
$$\frac{4\pi\alpha_s^2}{9s^2}[-\frac{(t-m_i^2)(t-m_j^2)+st}{(t-m_{\tilde{g}}^2)^2}-\delta_{ij}\frac{(u-m_i^2)(u-m_j^2)+su}{(u-m_{\tilde{g}}^2)^2}+$$

$$\frac{sm_{\tilde{g}}^2}{(t-m_{\tilde{g}}^2)^2}+\frac{sm_{\tilde{g}}^2}{(u-m_{\tilde{g}}^2)^2}\delta_{ij}-\frac{2sm_{\tilde{g}}^2}{3(t-m_{\tilde{g}}^2)(u-m_{\tilde{g}}^2)}\delta_{ij}]\,,$$

where m_i and m_j are the masses of produced squarks and $m_{\tilde{g}}$ is the gluino mass.

For the reaction $q_i\bar{q}_j \to \tilde{q}_i\tilde{q}_j^*$ the differential cross section has the form

$$\frac{d\sigma}{dt}(q_i\bar{q}_j \to \tilde{q}_i\tilde{q}_j^*) = \tag{200}$$
$$\frac{4\pi\alpha_s^2}{9s^2}[[\frac{ut-m_i^2m_j^2}{s^2}][\delta_{ij}[2-\frac{2}{3}\frac{s}{(t-m_{\tilde{g}}^2)}]+\frac{s^2}{(t-m_{\tilde{g}}^2)^2}]+\frac{sm_{\tilde{g}}^2}{(t-m_{\tilde{g}}^2)^2}]\,.$$

For the reaction $gg \to \tilde{q}_i\tilde{q}_i^*$ the differential cross section is

$$\frac{d\sigma}{dt}(gg \to \tilde{q}_i\tilde{q}_i^*) = \tag{201}$$
$$\frac{\pi\alpha_s^2}{s^2}[\frac{7}{48}+\frac{3(u-t)^2}{16s^2}][1+\frac{2m^2t}{(t-m^2)^2}+\frac{2m^2u}{(u-m^2)^2}+\frac{4m^4}{(t-m^2)(u-m^2)}]\,.$$

Here m is the mass of the corresponding squark (we assume the left- and right-handed squarks are degenerated in mass).

The differential cross section for the reaction $gq_i \to gaugino + \tilde{q}_i$ has the form

$$\frac{d\sigma}{dt}(gq_i \to gaugino + \tilde{q}_i) = \tag{202}$$
$$\frac{\pi}{s^2}[B_s\frac{(\mu^2-t)}{s}+B_t\frac{[(\mu^2-t)s+2\mu^2(m_i^2-t)]}{(t-\mu^2)^2}+$$
$$B_u\frac{(u-\mu^2)(u+m_i^2)}{(u-m_i^2)^2}+B_{st}\frac{[(s-m_i^2+\mu^2)(t-m_i^2)-\mu^2s]}{s(t-\mu^2)}+$$
$$B_{su}\frac{[s(u+\mu^2)+2(m_i^2-\mu^2)(\mu^2-u)]}{s(u-m_i^2)}+$$
$$B_{tu}[(m_i^2-t)(t+2u+\mu^2)+(t-\mu^2)(s+2t-2m_i^2)$$
$$+(u-\mu^2)(t+\mu^2+2m_i^2)]/2(t-\mu^2)(u-m_i^2)]\,,$$

where μ is the mass of the gauge fermion and m_i is the mass of the scalar quark. The coefficients B_x are contained in paper of E.Eichten et al. [4]. For instance, for the case when $gaugino \equiv gluino$ the coefficients B_x are: $B_s = \frac{4\alpha_s^2}{9}\delta_{ij}$, $B_t = \frac{9}{4}B_s$, $B_u = B_s$, $B_{st} = -B_t$, $B_{su} = \frac{1}{8}B_s$, $B_{tu} = \frac{9}{8}B_s$.

Consider finally the production of sleptons. The differential cross section for the production of charged slepton-sneutrino pairs is

$$\frac{d\sigma}{dt}(d\bar{u} \to W \to \tilde{l}_L\bar{\tilde{\nu}}_L) = \frac{g_2^4|D_W(s)|^2}{192\pi s^2}(tu-m_{\tilde{l}_L}^2m_{\tilde{\nu}_L}^2)\,. \tag{203}$$

For $\tilde{l}_L$ pair production the differential cross section is

$$\frac{d\sigma}{dt}(q\bar{q} \to \gamma^*, Z \to \tilde{l}_L\bar{\tilde{l}}_L) = \frac{2\pi\alpha^2}{3s^2}[tu - m^4_{\tilde{l}_L}][\frac{q_l^2 q_q^2}{s^2} + (\alpha_l - \beta_l)^2(\alpha_q^2 + \beta_q^2)|D_Z(s)|^2 + \frac{2q_l q_q \alpha_q(\alpha_l - \beta_l)(s - M_Z^2)}{s}|D_Z(s)|^2], \quad (204)$$

where $D_V(s) = 1/(s - M_V^2 + iM_V\Gamma_V)$, $q_l = -1$, $q_\nu = 0$, $q_u = 2/3$, $q_d = -1/3$, $\alpha_l = \frac{1}{4}(3t - c)$, $\alpha_\nu = \frac{1}{4}(c + t)$, $\alpha_u = -\frac{5}{12}t + \frac{1}{4}c$, $\alpha_d = -\frac{1}{4}c + \frac{1}{12}t$, $\beta_l = \frac{1}{4}(c + t)$, $\beta_\nu = -\frac{1}{4}(c + t)$, $\beta_u = -\frac{1}{4}(c + t)$, $\beta_d = \frac{1}{4}(c + t)$, $c = \cot\theta_W$, $t = \tan\theta_W$. The differential cross section for sneutrino pair production can be obtained by the replacement α_l, β_l, q_l and $m_{\tilde{l}}$ by α_ν, β_ν, 0 and $m_{\tilde{\nu}}$, respectively, whereas for $\tilde{l}_R$ pair production one has to substitute $\alpha_l - \beta_l \to \alpha_l + \beta_l$ and $m_{\tilde{l}_L} \to m_{\tilde{l}_R}$.

Superparticle Decays. The decay widths of the superparticles depend rather strongly on the relations between superparticle masses. Here we outline the main decay channels only. The formulae for the decay widths are contained in Refs. 49. Consider at first the decays of gluino and squarks. For $m_{\tilde{g}} > m_{\tilde{q}}$ the main decays are the following:

$$\tilde{g} \to \tilde{q}_i\bar{q}_i\,, \bar{\tilde{q}}_i q_i\,, \quad (205)$$

$$\tilde{q}_k \to \chi_i^0 q_k\,, \quad (206)$$

$$\tilde{q}_k \to \chi_j^+ q_m,\ \chi_j^- q_l\,. \quad (207)$$

For $m_{\tilde{g}} < m_{\tilde{q}}$ the main decays are:

$$\tilde{q}_i \to \tilde{g}q_i\,, \quad (208)$$

$$\tilde{g} \to q\bar{q}'\chi_k^+\,, \quad (209)$$

$$\tilde{g} \to q'\bar{q}\chi_k^-\,, \quad (210)$$

$$\tilde{g} \to q\bar{q}\chi_k^0\,. \quad (211)$$

The charginos and neutralinos usually are supposed to be lighter than gluino and squarks and their main decays are:

$$\chi_i^0 \to \chi_j^0 + Z\,, \quad (212)$$

$$\chi_i^0 \to \chi_j^\pm + W^\mp\,, \quad (213)$$

$$\chi_i^\pm \to \chi_j^0 + W^\pm\,, \quad (214)$$

$$\chi_i^\pm \to \chi_j^\pm + Z\,. \quad (215)$$

Two-body decays of neutralinos and charginos into Higgs bosons are:

$$\chi_i^0 \to \chi_j^0 + h(H)\,, \tag{216}$$

$$\chi_i^0 \to \chi_k^\pm + H^\mp\,, \tag{217}$$

$$\chi_i^\pm \to \chi_k^0 + H^\pm\,, \tag{218}$$

$$\chi_i^\pm \to \chi_j^\pm + h(H)\,. \tag{219}$$

The left sleptons dominantly decay via gauge interactions into charginos or neutralinos via two body decays

$$\tilde{l}_L \to l + \chi_i^0\,, \tag{220}$$

$$\tilde{l}_L \to \nu_L + \chi_j^-\,, \tag{221}$$

$$\tilde{\nu}_L \to \nu_L + \chi_i^0\,, \tag{222}$$

$$\tilde{\nu}_L \to l + \tilde{\chi}_j^+\,. \tag{223}$$

For relatively light sleptons only the decays into the LSP are possible, so that light sneutrino decays are invisible. Heavier sleptons can decay via the chargino or other (non LSP) channels. These decays are important because they proceed via the larger $SU(2)$ gauge coupling constant and can dominate the direct decay to LSP. The $SU(2)$ singlet charged sleptons $\tilde{l}_R$ only decay via their $U(1)$ gauge interactions and in the limit of vanishing Yukawa coupling their decays to charginos are forbidden. Therefore the main decay mode of right-handed slepton is

$$\tilde{l}_R \to l + \chi_i^0\,. \tag{224}$$

In many cases the mode into LSP dominates.

Let us now briefly describe the main signatures for the search for sparticles at LHC. Sparticle pair production at LHC is followed by sparticle decays untill the LSP is reached. Therefore, the main signature of sparticle production are the events with $(n \geq 0)$ jets plus $m \geq 0$ isolated leptons plus missing transverse energy due to escaping from detector registration 2 LSP. It is natural to divide the signatures into the following categories [50]:

a. multijets plus E_t^{miss} events,
b. 1l plus jets plus E_t^{miss} events,
c. 2l plus jets plus E_t^{miss} events,
d. 3l plus jets plus E_t^{miss} events,
e. 4l plus jets plus E_t^{miss} events,
f. $\geq 5l$ plus jets plus E_t^{miss} events.

Multileptons arise as a result of the cascade decays of neutralinos and charginos into W- and Z-bosons with subsequent decays of W- and Z-bosons

into leptonic modes. For instance, the same sign dilepton events arise as a result of the cascade decay

$$\tilde{g} \to q^{'}\bar{q}\chi^{\pm},\ \chi^{\pm} \to W^{\pm}\chi_1^0 \to l^{\pm}\nu\chi_1^0, \tag{225}$$

where l stands for both e and μ. Opposite sign dilepton events can arise as a result of cascade decay

$$\tilde{g} \to q\bar{q}\chi_i^0,\ \chi_i^0 \to Z\chi_1^0 \to l^+l^-\chi_1^0. \tag{226}$$

It should be noted that multilepton supersymmetry signatures arise as a result of decays of squarks or gluino into charginos or neutralinos different from LSP with subsequent decays of charginos or neutralinos into (W, Z)-bosons plus LSP. Leptonic decays of (W, Z)-bosons is the origin of leptons. However, for the case of nonuniversal gaugino mass relations at GUT scale it is possible to realize the situation [42] when all charginos and neutralinos are heavier than gluino and squarks. Therefore, gluino and squarks will decay mainly into quarks or gluons plus LSP, so cascade decays and as a consequence multilepton events will be absent.

3.3.2. The Search for SUSY Higgs Bosons

In MSSM there are four Higgs bosons ($h, H, A, H^{\pm}$). As it has been mentioned before at tree-level the lightest Higgs boson mass is predicted to be lighter than m_Z. However an account of radiative corrections for big top quark mass (that takes place in reality) can increase the Higgs boson mass up to 120 GeV for stop mass equal to 1 TeV. From the vacuum stability bound [15] the standard Higgs boson mass for $m_t \geq 175$ GeV is predicted to be heavier than 120 GeV. It means that the predictions for the Higgs boson mass in MSSM and SM lie in different mass intervals, i.e., the knowledge of the Higgs boson mass allows one to discriminate between MSSM and SM. In particular, the discovery of light Higgs boson at LEP2 will be powerful untrivial evidence in favour of low energy broken supersymmetry.

$h, H \to \gamma\gamma$. In the MSSM, the neutral Higgs boson remains extremely narrow in the kinematic region where the two photon decay has a reasonable branching ratio. The experimental requirements and backgrounds are the same as in the case of standard Higgs boson decaying into two photons. Therefore the ECAL mass resolution and acceptance are crucial for the Higgs boson discovery. For the case when SUSY masses are bigger than $O(300)$ GeV the branching of $h \to \gamma\gamma$ in MSSM coincides with the corresponding branching of SM, so we have in fact the same significance as in the case of SM. We shall consider the limiting case when the sparticle masses are heavy enough and they don't play important role in Higgs boson decays. So the decay channels for the MSSM lightest Higgs boson

are the same as for the SM Higgs boson, but the production rates are significantly modified by MSSM couplings. There are two main production processes for MSSM neutral Higgs bosons: $gg \to h(H)$ and $gg \to h(H)b\bar{b}$. The second mechanism is important at large $\tan\beta$ due to enhanced $h(H)b\bar{b}$ couplings. These associated production processes are interesting, as b-tagging techniques may be able to enhance the signal/background ratio, possibly allowing the observation of h, H and A [51].

$H \to ZZ^*, ZZ$ **and** $h \to ZZ^*$**.** The scalar Higgs bosons H and h couple to W- and Z-boson pairs, and so may be searched for in 4-lepton final states from $h, H \to ZZ^*, ZZ$. The regions of MSSM $(\tan(\beta), m_A)$-space $(\tan(\beta) = \frac{<H_t>}{<H_b>}$,m_A is the mass of the axial Higgs boson), where the Higgs bosons could be discovered through four lepton modes are divided into the region of low $\tan(\beta)$, where H could be discovered, and the high $\tan(\beta)$ region, where only h could be discovered.

$h, H, A \to \tau\bar{\tau} \to l^{\pm}h^{\pm} + X$**.** The $\tau\bar{\tau}$ final states can be searched for in a 'lepton + hadron' final state or in a $e + \mu$ final state. For the one lepton plus one hadron final states, intermediate backgrounds are due to $Z, \gamma^* \to \tau\bar{\tau}; t\bar{t} \to \tau\bar{\tau} + X, \tau + X$ and $b\bar{b} \to \tau\bar{\tau} + X, \tau X$. Reducible backgrounds are due to the events with one hard lepton and jets with a jet misidentified as a τ. Typically cuts are the following [1]:

1. One isolated lepton with $p_T \geq (15 - 40)$ GeV depending on the axial Higgs boson mass m_A and $|\eta| \leq 2$.
2. One τ-jet candidate which contains only one charged hadron.
3. No other significant jet activity.

An overall lepton reconstruction of 90 per cent is assumed. For the $\tau\bar{\tau} \to e^{\pm} + \mu^{\mp}$ final states a pair of opposite sign isolated electrons and muons with $p_T \geq 20$ GeV and $|\eta| \leq 2$ is required. There can be large backgrounds from $Z, \gamma^* \to \tau\bar{\tau}, t\bar{t}, b\bar{b}$ and W^+W^-. The $t\bar{t}$ and W^+W^- backgrounds can be reduced to the level of ≈ 20 per cent of the Z, γ^* backgrounds. Roughly speaking A, H-bosons can be discovered using these modes with the masses up to 600 GeV.

Charged Higgs $H^{\pm}$ **in** $t \to H^{\pm}h$, $H^{\pm} \to \tau\nu_{\tau}$**.** In the MSSM, the top quark can decay to a charged Higgs ($t \to H^+b$). The $t \to H^+b$ branching ratio is large at low and large $\tan(\beta)$ values, having a minimum at $\tan(\beta) \approx 6$. The H^+ has two main decay modes, $H^+ \to c\bar{s}$ and $H^+ \to \tau^+\nu_{\tau}$. The $H^+ \to \tau^+\nu_{\tau}$ branching is large for $\tan(\beta) \geq 2$, and only slightly depends on $\tan(\beta)$.

$h, H, A \to \mu^+\mu^-$**.** In the SM and in the MSSM for interesting values of the Higgs boson masses the branching ratio of $H \to \mu^+\mu^-$ is small $\approx 3 \cdot 10^{-4}$. For the SM Higgs boson the main background is the Drell-Yan production $\gamma*, Z \to \mu^+\mu^-$. However, in the MSSM the $\mu^+\mu^-$-channel could be very interesting for

large values of $\tan(\beta)$. It appears that for $m_A \leq 200$ GeV and $\tan(\beta) \geq 2.5$ for integrated luminosity 10^4pb^{-1} it is possible to discover A- and H-bosons at the level $\geq 7\sigma$. The discovery potential of the Higgs boson for this mode at $L = 10^5$ pb^{-1} is similar to the discovery potential of the Higgs boson for the standard mode $H, h, A \to \tau\tau$ for 10^4pb^{-1}. However the $\mu^+\mu^-$-channel gives a much better signal identification and mass resolution [1].

h,H,A in Associated Production $\bar{b}bH_{susy}$. Whilst the $gg \to b\bar{b}H$ associated production is negligible for the SM Higgs boson compared to $t\bar{t}H$ in the MSSM, the rate of $gg \to b\bar{b}H_{susy}$ is (30 - 50) per cent of the total production for $m_A = 100$ GeV and (70 - 80) per cent for $m_A = 300$ GeV with $\tan(\beta) = 10-30$. The signal-to-background ratio can be enhanced by b-tagging.

$A \to Zh \to b\bar{b}b\bar{b}$. The large branching ratio (≈ 50 per cent) of $A \to Zh$ in the region $\tan(\beta) \leq 2$ for 180 GeV$\leq m_A \leq 2m_t$ could allow the observation of A and h in this region.

The main conclusion [1] concerning the situation with the search for MSSM Higgs bosons for different $(m_A, \tan(\beta))$ values is that Higgs bosons for $m_A \leq$ 500 GeV would be detectable at CMC except, maybe, very difficult region for 110 GeV$\leq m_A \leq$200 GeV, $3 \leq \tan(\beta) \leq 10$ and a smaller one for $\tan(\beta) \approx 2.5$ and 200 GeV $\leq m_A \leq$ 280 GeV. The most promising channel for these regions is $h, H \to \bar{b}b$, from Wh, Zh and $t\bar{t}h$ final states.

3.3.3. Squark and Gluino Search

Jets + E_T^{miss} Channel. There are a lot of possible scenario which depend on the concrete values of squark and gluino masses for the search for squarks and gluino using this signature. Consider two typical scenario [1].

Scenario A. : $m_{\tilde{b}}, m_{\tilde{t}} \leq m_{\tilde{g}}$.

In this case the two-body decay $\tilde{g} \to \tilde{b}\bar{b}$ with $\tilde{b} \to \chi_1^0 b$ dominates, because the top is too massive to allow $\tilde{g} \to t\bar{t}$ decay. Thus the resulting event signature will have 4 b-jets in final state.

Scenario B. : $m_{\tilde{q}} = m_{\tilde{g}}$.

For such scenario the gluino decays directly into LSP ($\tilde{g} \to q\bar{q}\chi_1^0$) leading to the typical $E_T^{miss} + multijets$ final state event topology without an excess of b-jets.

In scenario with heavy squarks and gluino ($m_{\tilde{q}} = 1550$ GeV, $m_{\tilde{g}} = 1500$ GeV) after using some cuts we have $\frac{N_{ev}}{N_{back}} \sim 8.5$. In general for an integrated luminosity of $10^5(\text{pb}^{-1} - 10^3\text{pb}^{-1})$, the sensitivity to the channel of multijets + missing energy can be expressed as a mass reach for gluino mass $m_{\tilde{g}}$ [2]:

$m_{\tilde{g}} \leq 1600(1050)$ GeV for $m_{\tilde{q}} = 2m_{\tilde{g}}$,
$m_{\tilde{g}} \leq 2300(1800)$ GeV for $m_{\tilde{q}} = m_{\tilde{g}}$,

$m_{\tilde{g}} \leq 3600(2600)$ GeV for $m_{\tilde{q}} = \frac{m_{\tilde{g}}}{2}$.

Lepton(s) + E_t^{miss} + Jets. Cascade decays of squarks and gluino are an important source of leptons. Therefore, events with E_t^{miss} + jets + lepton(s) provide a good signature for searching for gluinos and squarks over a wide mass range. Four event classes, containing one to three leptons (muons or electrons), give important signatures for the search for squarks and gluino:

$1l$: a single lepton + E_t^{miss} + jets,

$2l$: two leptons with opposite charges + E_t^{miss} + jets,

$2l(ss)$: same-sign dileptons + E_t^{miss} + jets,

$3l$: three dileptons + E_t^{miss} + jets.

The background comes from $t\bar{t}$, W + jets, Z + jets, WW, WZ. The main conclusion [52] is that the signature with a single lepton + E_t^{miss} gives the most powerful restriction on the gluino mass for the search for SUSY at CMS detector. Namely, for L_t from 10^4 pb^{-1} to 10^5 pb^{-1} the CMS will be able to discover gluino from 1.5 TeV up to 2 TeV and squarks from 1.5 TeV up to 2.3 TeV. Other conclusion is that the gluino and squark discovery mass limits are not very sensitive to the increase of SM background.

3.3.4. Neutralino and Chargino Search

Chargino and neutralino pairs, produced through the Drell-Yan mechanism or squark exchange, may be detected through their leptonic decays $\chi_1^{\pm}, \chi_2^0 \to lll + E_T^{miss}$. The leptonic decays of $\chi_1^{\pm}$ and χ_2^0 are the following:

$$\chi_1^{\pm} \to \chi_1^0 l^{\pm} \nu \ ,$$
$$\chi_1^{\pm} \to (\tilde{l}_{L,R}^{\pm} \to \chi_1^0 l^{\pm}) \nu \ ,$$
$$\chi_1^{\pm} \to (\tilde{\nu}_L \to \chi_1^0 \nu) l^{\pm} \ ,$$
$$\chi_1^{\pm} \to (W^{\pm} \to l^{\pm} \nu) \chi_1^0 \ ,$$
$$\chi_2^0 \to \chi_1^0 l^+ l^- \ ,$$
$$\chi_2^0 \to (\tilde{l}_{L,R}^{\pm} \to \chi_1^0 l^{\pm}) l^{\mp} \ ,$$
$$\chi_2^0 \to (\chi_1^{\pm} \to \chi_1^0 l^{\pm} \nu) l^{\mp} \nu \ .$$

The three-lepton signal is produced through the decay chain $\chi_1^{\pm} \to l^{\pm} + \chi_1^0$ and $\chi_2^0 \to ll + \chi_1^0$, where the undetected neutrino and χ_1^0 produce E_T^{miss}. The main backgrounds to this channel arise from WZ/ZZ, $t\bar{t}$, $Zb\bar{b}$ and $b\bar{b}$ production. In principle there could be SUSY background arising as a result of squark and gluino cascade decays into multileptonic modes.

Typical cuts are the following [53]:

i. Three isolated leptons with $p_t^l > 15$ GeV.

ii. Veto central jets with $E_t > 25$ GeV in $|\eta| < 3.5$.

iii. $m_{l\bar{l}} < 81$ GeV or $m_{l\bar{l}} \neq M_Z \pm \delta M_Z$.

The main conclusion is that neutralino and chargino could be detected provided their masses are lighter than 350 GeV [53]. Moreover, it is possible to determine the $M(\chi_2^0) - M(\chi_1^0)$ mass difference by the measurement of the distribution on l^+l^- invariant mass arising as a result of the decay $\chi_2^0 \to \chi_1^0 + l^+l^-$ [53].

3.3.5. Sleptons Search

Slepton pairs, produced through the Drell-Yan mechanism can be detected through their leptonic decays $\tilde{l} \to l + \chi_1^0$. So in the final state we expect dilepton pair with missing energy and no hadronic jets. Here we shall use the results of Ref. 54, where concrete estimates have been made for CMS detector. Namely, we consider two points of Ref. 54.

Point A: $m(\tilde{l}_L) = 314$ GeV, $m(\tilde{l}_R) = 192$ GeV, $m(\tilde{\nu}) = 308$ GeV, $m(\tilde{\chi}_1^0) = 181$ GeV, $m(\tilde{\chi}_2^0) = 358$ GeV, $m(\tilde{g}) = 1036$ GeV, $m(\tilde{q}) = 905$ GeV, $\tan(\beta) = 2$, $sign(\mu) = -$.

Point B: $m(\tilde{l}_L) = 112$ GeV, $m(\tilde{l}_R) = 98$ GeV, $m(\tilde{\nu}) = 93$ GeV, $m(\tilde{\chi}_1^0) = 39$ GeV, $m(\tilde{\chi}_2^0) = 87$ GeV, $m(\tilde{g}) = 254$ GeV, $m(\tilde{q}) = 234$ GeV, $\tan\beta = 2$, $sign\mu = -$.

For point A the following cuts have been used: $p_t^l \geq 50$ GeV, $Isol \leq 0.1$, $|\eta| \leq 2.5$, $E_t^{miss} \geq 120$ GeV, $\Delta\phi(E_t^{miss}, ll) \geq 150^o$, jet veto - no jets with $E_t^{jet} \geq 30$ GeV in $|\eta| \leq 4.5$, Z-mass cut - ($M_Z \pm 5$ GeV excluded), $\Delta\phi(l^+l^-) \leq 130^o$.

With such cuts for the total luminosity $L_t = 10^5 \text{pb}^{-1}$ 91 events with $e^+e^- + \mu^+\mu^-$ resulting from slepton decays have been found. The standard WS model background comes from WW, $t\bar{t}$, $Wt\bar{b}$, WZ $\tau\bar{\tau}$ and gives 105 events. No SUSY background have been found. The significance $S = \frac{Sleptons}{\sqrt{Background + Sleptons}}$ for the slepton discovery at the point A is $S = 6.5$.

For the point B the cuts are similar to the point A, except $p_l^t \geq 20$ GeV, $E_t^{miss} \geq 50$ GeV, $\Delta\phi(E_t^{miss}, ll) \geq 160^o$. For the total luminosity $L_t = 10^4 \text{pb}^{-1}$ the number of $e^+e^- + \mu^+\mu^-$ events resulting from direct slepton production has been found to be 323. The number of the background events has been estimated equal to 989 (standard model background) + 108 (SUSY background) = 1092. The significance is equal to $S = 8.6$.

The main conclusion of Ref. 54 is that for $L_t = 10^5 \text{pb}^{-1}$ CMS will be able to discover sleptons with the masses up to 400 GeV.

The Search for Flavour Lepton Number Violation in Slepton Decays. In supersymmetric models with explicit flavour lepton number violation due to soft supersymmetry breaking terms there could be detectable flavour lepton number violation in slepton decays [55]. For instance, for the case of nonzero mixing $\sin\phi \neq 0$ between right-handed selectrons and smuons we have flavour lepton

number violation in slepton decays, namely [55]:

$$\Gamma(\tilde{\mu}_R \to \mu + LSP) = \Gamma \cos^2 \phi\,, \tag{227}$$

$$\Gamma(\tilde{\mu}_R \to e + LSP) = \Gamma \sin^2 \phi\,, \tag{228}$$

$$\Gamma(\tilde{e}_R \to e + LSP) = \Gamma \cos^2 \phi\,, \tag{229}$$

$$\Gamma(\tilde{e}_R \to \mu + LSP) = \Gamma \sin^2 \phi\,, \tag{230}$$

$$\Gamma = \frac{g_1^2}{8\pi}(1 - \frac{M_{LSP}^2}{M_{SL}^2})^2\,. \tag{231}$$

The typical prediction of the nonzero smuon-selectron mixing is the existence of accoplanar $e^{\pm}\mu^{\mp}$ signal events with missing energy arising as a result of the production of slepton pairs with their subsequent decays with flavour lepton number violation. The possibility of detecting flavour lepton number violation in slepton decays at LHC has been discussed in Ref. 56. The main conclusion is that for the most optimistic case of the maximal mixing $\sin\phi = \frac{1}{\sqrt{2}}$ it would be possible to discover slepton mixing at LHC for the points A and B which have been considered for the case of zero slepton mixing in Ref. 54.

3.4. The Search for Physics beyond SM and MSSM

Search for New Vector Bosons. Many string inspired supersymmetric electroweak models and grand unified models based on extended gauge groups ($SO(10)$, E_6...) predict the existence of new relatively light neutral $Z^{'}$-bosons. The main mechanism for the production of such new neutral vector bosons is the quark-antiquark fusion. The cross section is given by the standard formula:

$$\sigma(pp \to Z^{'} + ...) = \sum_i \frac{12\pi^2 \Gamma(Z^{'} \to \bar{q}_i q_i)}{9 M_{Z^{'}} s} \int_{M_{Z^{'}}^2/s}^1 \frac{dx}{x} \tag{232}$$
$$[\bar{q}_{pi}(x,\mu) q_{pi}(x^{-1} M_{Z^{'}}^2 s^{-1}, \mu) + q_{pi}(x,\mu) \bar{q}_{pi}(x^{-1} M_{Z^{'}}^2 s^{-1}, \mu)\,.$$

Here $\bar{q}_{pi}(x,\mu)$ and $q_{pi}(x,\mu)$ are the parton distributions of the antiquark $\bar{q}_i$ and quark q_i in the proton at the normalization point $\mu \sim M_{Z^{'}}$, and $\Gamma(Z^{'} \to \bar{q}_i q_i)$ is the hadronic decay width of the $Z^{'}$-boson into quark-antiquark pair with a flavor i. In most models as a consequence of the γ_5 anomaly cancellation $Z^{'}$-boson interacts both with quarks and leptons, therefore the best signature for the search for $Z^{'}$-boson is through its decay to electron pairs, muon pairs and jet pairs. The LHC $Z^{'}$-boson discovery potential depends on the couplings of $Z^{'}$-boson with quarks and leptons. For the $Z^{'}$-boson decaying into lepton pair the main background comes from the Drell-Yan process which is under control. For

$Z^{'}$ with quark and lepton couplings equal to Z-couplings with quarks and leptons, it would be possible to discover the $Z^{'}$-boson with a mass up to 5 TeV [2].

Many extended gauge electroweak models based for instance on the gauge group $SU(2)_L \otimes SU(2)_R \otimes U(1)$ predict the existence of the additional charged vector $W^{'}$-boson. The main production mechanism for the $W^{'}$-boson is the quark-antiquark fusion similar to the case of $Z^{'}$-production. The best way to look for $W^{'}$-boson is through its leptonic mode $W^{'} \to l\nu$.

For the model with right-handed charged $W^{'}$-boson it would be possible to discover the $W^{'}$-boson through leptonic mode $W^{'} \to e\nu$ with $W^{'}$ mass up to 6 TeV [2]. Typical accuracy in the determination of the $W^{'}$-mass is (50 -100) GeV.

Search for Supesymmetry with R-Parity Violation. Most of supersymmetric phenomenology assumes the MSSM which conserves R-parity. As a consequence of R-parity conservation, supersymmetric particles can only be produced in pairs and a supersymmetric state cannot decay into conventional states. This has untrivial consequence for the search for supersymmetric particles at supercolliders; in particular all experimental searches of SUSY rely on pair production and on missing transverse momentum p_t^{miss} as a signal for the production of the LSP, which must be stable and electrically neutral. However, at present there are no deep theoretical motivations in favour of R-parity conservation. The phenomenology of the models with explicit R-violation at hadron colliders has been studied in Refs. 57. The most general trilinear terms in superpotential explicitly violating R-parity have the form [57]

$$W_{R,br} = \lambda_{ijk} L_i L_j \bar{E}_k + \lambda^{'}_{ijk} L_i Q_j \bar{D}_k + \lambda^{''}_{ijk} \bar{U}_i \bar{D}_j \bar{D}_k \,, \qquad (233)$$

where L and $\bar{E}$ (Q and $\bar{U}$, $\bar{D}$) are the (left-handed) lepton doublet and the antilepton singlet (quark doublet and antiquark singlets) chiral superfields, respectively. The terms of (233) violate baryon and lepton number and, if present in the Lagrangian, they generate an unacceptably large amplitude for proton decay suppressed only by the inverse squark mass squared. The R-parity prohibits the dangerous terms (233) in the superpotential. However, R-parity is not the single way to construct a minimal supersymmetric extension of the standard model. It is easy to write down alternative to R-parity symmetries which allow for a different set of couplings. For example, under the transformation

$$(Q, \bar{U}, \bar{D}) \to -(Q, \bar{U}, \bar{D}), \quad (L, \bar{E}, H_{1,2}) \to +(L, \bar{E}, H_{1,2}) \,, \qquad (234)$$

only the quark superfields change sign. If the Lagrangian is invariant under transformations (234), then only the last, baryon number violating term in (233) $\bar{U}\bar{D}\bar{D}$ is forbidden. This gives a new model in which a single supersymmetric state can couple to standard model states breaking R-parity. Similarly, there are analogous transformations forbidding the lepton number violating terms.

In the direct search for supersymmetric particles the phenomenology is altered considerably when including R-parity violating terms in the superpotential. In general both the production mechanisms and the decay patterns can change. Other than the standard supersymmetric pair production of particles there is now the possibility of producing R-odd final states as well. Also, if all supersymmetric particles decay in the detector, we will no longer have the standard p_t^{miss} signal and the decay patterns will all be altered. In particular, the LSP will decay mainly into three-body final states [57]. However, except for LSP, which now decays, all particles predominantly decay as in the MSSM. Consider the case when LSP decays within the detector. For the model with R-parity breaking terms involving leptonic superfields we expect additional lepton pairs in the final state as a result of the LSP decay. Therefore we expect instead of missing energy signature the presence of additional lepton pairs compared to standard MSSM signatures that is in principle more visible at LHC than the SUSY signatures in MSSM. The $\bar{U}\bar{D}\bar{D}$ operators however lead to less characteristic signals, but for cascade decays they lead to signals comparable to those in the MSSM.

Note that it is possible to construct the model with supersmall R-parity violation and with relatively longlived $t \sim (10^{-1} - 10^{-9})$ s charged $\tilde{\tau}_R$ slepton playing the role of LSP [59]. Relatively longlived charged LSP penetrates through the detector and it is possible to detect it by the track measurement.

Search for Leptoquarks. At LHC the leptoquark pair production proceeds dominantly through gg-fusion, which does not involve any lepton-quark-leptoquark vertex and therefore is predicted with $\approx$ 50 per cent accuracy. In 25 per cent of the events, the final state contains 2 electrons and 2 jets. The dominant background in this case is from $t\bar{t}$ production. The conclusion is that leptoquarks with masses up to 1 TeV will be discovered at LHC.

Search for Scalar Colour Octets. Relatively light ($M_8 \leq O(1)$ TeV) scalar $SU_c(3)$ colour $SU_L(2) \otimes U(1)$ neutral octets are predicted in some supersymmetric and nonsupersymmetric GUTs [59]. Light scalar octets naturally arise in models with big compactification radius of the additional space dimensions.

To be precise, consider light scalar octets neutral under $SU_L(2) \otimes U(1)$ electroweak gauge group. Such particles are described by the selfconjugate scalar field $\Phi^\alpha_\beta(x)$ ($(\Phi^\alpha_\beta(x))^* = \Phi^\beta_\alpha(x), \sum_\alpha \Phi^\alpha_\alpha(x) = 0$) and they interact only with gluons. Here $\alpha = 1, 2, 3$; $\beta = 1, 2, 3$ are the $SU(3)$ indices. The scalar potential for the scalar octet field $\Phi^\alpha_\beta(x)$ has the form

$$V(\Phi) = \frac{M^2}{2} Tr(\Phi^2) + \frac{\lambda_1 M}{6} Tr(\Phi^3) + \frac{\lambda_2}{12} Tr(\Phi^4) + \frac{\lambda_3}{12} (Tr(\Phi^2))^2 . \quad (235)$$

The term $\frac{\lambda_1 M}{6} Tr(\Phi^3)$ in the scalar potential (235) breaks the discrete symmetry $\Phi \to -\Phi$. The existence of such term in the Lagrangian leads to the decay of scalar octet mainly into two gluons through one-loop diagrams similar to

the corresponding one-loop diagrams describing the Higgs boson decay into two photons. One can find that the decay width of the scalar octet into two gluons is determined by the formula [60]

$$\Gamma(\Phi \to gg) = \frac{15}{4096\pi^3}\alpha_s^2 c^2 \lambda_1^2 M\,, \tag{236}$$

where

$$c = \int_0^1 \int_0^{1-w} du\, dw\, \frac{wu}{1-u-w} \simeq 0.48 \tag{237}$$

and α_s is the effective coupling constant at some normalization point $\mu \sim M$. Numerically for $\alpha_s = 0.12$ we find that

$$\Gamma(\Phi \to gg) = 0.4 \cdot 10^{-8} \lambda_1^2 M\,. \tag{238}$$

From the requirements that colour $SU(3)$ symmetry is unbroken (the minimum $< \Phi_\beta^\alpha(x) >= 0$ is the deepest one) and the effective coupling constants $\bar{\lambda}_2$, $\bar{\lambda}_3$ don't have Landau pole singularity up to the energy $M_o = 100M$ we find that $\lambda_1 \leq O(1)$. Therefore the decay width of the scalar colour octet is less than $O(1)$ KeV, $O(10)$ KeV for the octet masses 100, 1000 GeV, respectively. It means that new hadrons composed from scalar octet Φ, quarks and gluons ($g\Phi$, $\bar{q}\Phi q$, $qqq\Phi$) are relatively longlived even for high scalar octet mass. Consider the pair production of scalar octets at LHC. The corresponding lowest order parton cross sections have the form [60]

$$\frac{d\sigma}{dt}(\bar{q}q \to \Phi\Phi) = \frac{4\pi\alpha_s^2}{3s^4}(tu + M^4)\,, \tag{239}$$

$$\frac{d\sigma}{dt} = \frac{\pi\alpha_s^2}{s^2}\left(\frac{81}{96} + \frac{9(u-t)^2}{32s^2}\right)\left(1 + \frac{2M^2}{u-M^2} + \frac{2M^2}{t-M^2} + \frac{2M^4}{(u-M^2)^2} + \frac{2M^4}{(t-M^2)^2} + \frac{4M^4}{(t-M^2)(u-M^2)}\right), \tag{240}$$

$$\sigma(\bar{q}q \to \Phi\Phi) = \frac{2\pi\alpha_s^2}{9s}k^3\,, \tag{241}$$

$$\sigma(gg \to \Phi\Phi) = \frac{\pi\alpha_s^2}{s}\left(\frac{15k}{16} + \frac{51kM^2}{8s} + \frac{9M^2}{2s^2}(s-M^2)\ln\left(\frac{1-k}{1+k}\right)\right), \tag{242}$$

where $k = (1 - \frac{4M^2}{s})^{\frac{1}{2}}$. At LHC the main contribution ($\geq$ 95 per cent) for the production of scalar octets comes from the gluon annihilation into two scalar octets $gg \to \Phi\Phi$. The scalar octets decay into two gluons that leads to the four-jet events at LHC. Therefore the single signature of the scalar octets at LHC are the

four-jet events. The main background comes from QCD four-jet events. The cross section for the scalar octet production is typically $O(10^{-4})$ of the standard QCD two-jet cross section and it is $O(10^{-2})$ of the four-jet QCD background. The preliminary conclusion is that at LHC for $L_t = 10^5$ pb^{-1} it would be possible to discover the scalar octets with the mass $M \leq 900$ GeV.

Search for Kaluza-Klein States. As is well known, new degrees of freedom are required in any attempt of unification of the electroweak and strong interactions with gravity. Among these attempts only superstring theory is known to provide a consistent description of quantum gravity. Strings predict two kinds of new degrees of freedom:

(i) Superheavy oscillation modes whose characteristic scale is given by the inverse string tension $(\alpha')^{-\frac{1}{2}} \sim 10^{18}$ GeV. These states are important at very short distances of the order of Planck length and modify the ultraviolet behavior of gravitational interactions.

(ii). States associated to the internal compactified space whose presence is required from the fact that superstring theory in flat space is anomally free only in ten dimensions. Usually, the size of the internal space is also made too small to give any observable effect in particle accelerators.

However it is possible to construct superstring models having one or two large internal dimensions at a scale accessible to LHC [61]. The presence of such large dimensions is motivated by superstring theory with perturbative breaking of supersymmetry [62] and their size is inversely proportional to the scale of supersymmetry breaking which must be of the order of the electroweak scale in order to protect the gauge hierarchy. In contrast to field theoretical expectations, string theory allows the existence of such large dimension(s) consistently with perturbative unification of low-energy couplings in a class of models based on orbifold compactifications [63]. Properties of string models with perturbative breaking of supersymmetry, were studied in the case of minimal embedding of the standard model [64]. The main signature of the large extra dimension(s) in these constructions is the appearance of a tower of excitations for the gauge bosons and Higgs bosons with the same gauge quantum numbers. The Kaluza-Klein(KK) states are the straightforward consequence of all models with compactified dimensions and they have masses:

$$m_n^2 = m_0^2 + \frac{\vec{n}^2}{R^2}\,, \tag{243}$$

where R denotes the common radius of the D large internal dimensions, $\vec{n}$ is a D-dimensional vector and m_0 denotes for R-independent contributions coming from the electroweak symmetry breaking. All massive KK-states are unstable and they decay into quarks and leptons with a lifetime $O(10^{-26})$ s when the size of the compact dimension(s) is $O(1)$ TeV^{-1}. Present experimental limits have been obtained from an analysis of the effective four-fermion operators which arise

from the exchange of the massive KK-modes [65]. In orbifold models the current limits are $R^{-1} \geq 185$ GeV for one large extra dimension, while $R^{-1} \geq 1.4$ TeV, 1.1 TeV, 1 TeV for two large dimensions in the case of Z_3, Z_4, and Z_6 orbifolds, respectively [66].

Among the KK-excitations of different spins, the easiest way to detect at LHC are the vectors with the quantum numbers of the electroweak $SU_L(2) \otimes U(1)$ gauge bosons. The most efficient way of observing KK-states in proton-proton collisions is to identify charged leptons $l^{\pm}$ in the final state. The main background comes from the Drell-Yan process $pp \to l^+l^- + X$ with $l = e, \mu$. In many models with large compactified dimension(s) due to accidental suppression of the effective coupling constant of the massive $SU(2)$ vector excitations, only the $U(1)$ vector excitations couple to leptons. These states have masses given by equation (243) and they couple with fermions through the effective interaction:

$$g'^*(p)\bar{\psi}^k \gamma_\mu (v_k + a_k \gamma_5) \psi^k B_n^{*\mu}\,, \tag{244}$$

where k labels the different species of fermions, and $g'^*(p)$ is an effective coupling constant at scale p. The interaction (244) leads to rates of N_n^*-decays into fermions:

$$\Gamma(B_n^* \to f\bar{f}) = (g'^*(m_n))^2 \frac{m_n}{12\pi} C_f (v_f^2 + a_f^2)\,, \tag{245}$$

while the corresponding interaction with their scalar superpartners $\tilde{f}_{R,L}$ leads to the decay rates

$$\Gamma(B_n^* \to \bar{\tilde{f}}_{R(L)} \tilde{f}_{R(L)}) = (g'^*(m_n))^2 \frac{m_n}{48\pi} C_f (v_f \pm a_f)^2\,, \tag{246}$$

where $C_f = 1$ or 3 for colour singlets or triplets, respectively. The total width is:

$$\Gamma_n = \frac{5}{8\pi} (g'^*)^2 m_n\,. \tag{247}$$

The total cross section for the production of the KK-excitations B_n^* is given by [61]

$$\sigma_t = \sum_{quarks} \int_0^{\sqrt{s}} dM \int_{\ln M/\sqrt{s}}^{\ln \sqrt{s}/M} dy\, q_q(y, M) S_q(y, M)\,, \tag{248}$$

where

$$g_q(y, M) = \frac{M}{18\pi} x_a x_b [f_q^{(p)}(x_a, M) f_{\bar{q}}^{(p)}(x_b, M) + f_{\bar{q}}^{(p)}(x_a, M) f^{(b)}(x_b, M)]\,, \tag{249}$$

and

$$S_q(y, M) = (g'^*)^4 \frac{1}{N} \sum_{|\vec{n}| < R\sqrt{s}} \frac{(v_q^2 + a_q^2)(v_l^2 + a_l^2)}{(M^2 - m_n^2)^2 + \Gamma_n^2 m_m^2}\,, \tag{250}$$

where $x_a = \frac{M}{\sqrt{s}} e^y$, $x_b = \frac{M}{\sqrt{s}} e^{-y}$, factor N comes from Z_N orbifold projection. The main background comes from the Drell-Yan production mechanism. The main conclusion of Ref. 60 is that at LHC for $L_t = 10^5$ pb^{-1} it would be possible to obtain a bound $R^{-1} \geq 4.5$ TeV on the compactification radius.

Compositeness. A composite structure for quarks would appear in the form deviations from the standard QCD expectations at high transverse momenta, where valence quark scattering dominates. It is expected that it would be possible to discover the quark compositeness scale with $\Lambda_c \leq 10$ TeV. The best way to look for the lepton compositeness effects is the study of lepton pair production at large dilepton invariant masses. It would be possible to discover the lepton compositeness for $\Lambda_{lept} \leq 20$ TeV [2].

Nonstandard Higgs Bosons. Many-Higgs doublet model where each Higgs doublet couples with its own quark with relatively big Yukawa coupling constant has been considered in Ref. 66. For nonsmall Yukawa coupling constants the main reaction for the production of the Higgs doublets corresponding to the first and the second generations is quark-antiquark fusion. The phenomenology of the Higgs doublets corresponding to the third generation is very similar to the phenomenology of the model with two Higgs doublets. The cross section for the quark-antiquark fusion in quark-parton model in the approximation of the infinitely narrow resonances is given by the standard formula

$$\sigma(AB \to H_{q_i q_j} + X) = \frac{4\pi^2 \Gamma(H_{q_i q_j} \to \bar{q}_i q_j)}{9 s M_H} \int_{\frac{M_H^2}{s}}^1 \frac{dx}{x} \tag{251}$$
$$[\bar{q}_{Ai}(x,\mu) q_{Bj}(x^{-1} M_H^2 s^{-1}, \mu) + q_{Aj}(x,\mu) \bar{q}_{Bj}(x^{-1} M_H^2 s^{-1}, \mu)] .$$

Here $\bar{q}_{Ai}(x,\mu)$ and $q_{Aj}(x,\mu)$ are parton distributions of the antiquark $\bar{q}_i$ and quark q_j in hadron A at the normalization point $\mu \sim M_H$ and the $\Gamma(H_{q_i q_j} \to \bar{q}_i q_j)$ is the hadronic decay width of the Higgs boson into quark-antiquark pair. For the Yukawa Lagrangian

$$L_Y = h_{q_i q_j} \bar{q}_{Li} q_{Rj} H_{q_i q_j} + h.c. , \tag{252}$$

the hadronic decay width for massless quarks is

$$\Gamma(H_{q_i q_j} \to \bar{q}_i q_j) = \frac{3 M_H h_{q_i q_j}^2}{16\pi} . \tag{253}$$

The value of the renormalization point μ has been chosen equal to the mass M_H of the corresponding Higgs boson. The variation of the renormalization point μ in the interval $0.5 M_H - 2 M_H$ leads to the variation of cross section less than 50 per cent. In considered models there are Higgs bosons which couple both with down quarks and leptons, so the best signature is the search for the electrically neutral Higgs boson decays into e^+e^- or $\mu^+\mu^-$ pairs. For the charged

Higgs bosons the best way to detect them is to look for their decays into charged leptons and neutrino. The Higgs doublets which couple with up quarks in model with massless neutrino do not couple with leptons, so the only way to detect them is the search for the resonance type structure in the distribution of the dijet cross section on the dijet invariant mass as in the case of all Higgs bosons, since in the considered models all Higgs bosons decay mainly into quark-antiquark pairs that leads at the hadron level to additional dijet events. However the accuracy of the determination of the dijet cross section is $O(10)$ per cent, so it would be not so easy to find stringent bound on the Higgs boson mass by the measurement of dijet differential cross section at LHC. In considered many Higgs doublet model, due to the smallness of the vacuum expectation values of the Higgs doublets corresponding to the u-, d-, s-, and c-quarks, after electroweak symmetry breaking the mass splitting inside the Higgs doublets is small, so in such models the search for neutral Higgs boson decaying into lepton pair is in fact the search for the corresponding Higgs isodoublet. The main background in the search for neutral Higgs bosons through their decays into lepton pair is the Drell-Yan process which is under control. The main conclusion of Ref.66 is that at LHC for $L_t = 10^5$ pb^{-1} and for the corresponding Yukawa coupling constant $h_Y = 1$ it would be possible to detect such Higgs bosons with the masses up to $4.5 - 5$ TeV.

Search for Vector-Like Fermions. Vector-like fermions are characterized by having their left- and right-handed components transforming in the same way under the gauge symmetry group. Therefore their mass terms $\bar{\psi}_L \psi_R$ are not forbidden by any symmetry. As a consequence their masses are unbounded and they decouple when they are taken to infinity. The standard model does not need vector-like fermions and the models with additional vector-like fermions are not very popular at present. Vector-like fermions decay by the exchange of standard electroweak gauge and Higgs bosons , $W^{\pm}$, Z, h, with all three being comparable in size [67]. It is possible to add to standard model extra vector-like fermions with the following quantum numbers:

a. Down singlet D-quark.
b. Up singlet U-quark.
c. Up down quark doublet (U, D)
d. Singlet charged lepton E.
e. Singlet neutral lepton N.
f. Neutral charged lepton doublet (N, E).

The production cross sections are similar to those of standard fermions.

Vector-like quarks decay mainly into $Q \to Wq_i$, Zq_i, hq_i modes, while vector-like leptons decay mainly into $L \to Wl$, Zl, hl modes. For vector-like quarks the branchings obey the approximate rule: $W/Z/h \approx 2/1/1$. The signatures from vector-like quark pair production at LHC with their subsequent decays are: 6-jets events, 2-leptons + 4-jets events and 4-leptons + 2-jets events. The sig-

natures from the vector-like lepton pair production with their subsequent decays are: 6-leptons events, 4-leptons + 2-jets events, 2-leptons + 4-jets events.

4. CONCLUSION

LHC can test the structure of many theories at TeV scale. LHC will be able to discover Higgs boson and low energy broken supersymmetry with squark and gluino masses up to (2 - 2.5) TeV. Also there is nonzero chance to find something new (Z'-bosons, W'-bosons, leptoquarks...) at LHC. At any rate after LHC we will know the basic elements of the matter structure at TeV region.

We are indebted to our colleagues from INR Theoretical Department for useful discussions. The research described in this publication was made possible in part by Award No.RP1-187 of the U.S. Civilian Research and Development Foundation for the Independent States of the Former Soviet Union (CRDF).

REFERENCES

1. CMS, Technical Proposal, CERN/LHCC/94-38 LHCCP1, December 15, 1994.
2. ATLAS, Technical Proposal, CERN/LHCC/94-43 LHCCP2, December 15, 1994.
3. **Berman S.M., Bjorken J.D., Kogut J.B.** — Phys.Rev., 1971, v.D4, p.3388.
4. See for example: **R.P.Feynman** — Photon-Hadron Interactions (Benjamin, Reading, Massachusetts) 1972;
   Eichten E., Hinchlife I., Lane K., Quigg C. — Rev.Mod.Phys., 1984, v.56, p.579; 1986, v.E58, p.1065.
5. See for example: **Dokshitzer Yu.L., Khoze V.A., Mueller A.H. Troyan S.I.** — Basics of Perturbative QCD, Editions, Frontiers, Gif-sur-Yvette, 1991;
   Altarelli G. — Phys.Rep., 1981, v.81, p.1;
   Bassetto A., Ciafaloni M., Marchesini G. — Phys.Rep., 1983, v.C100, p.201.
6. **Botts J. et al.** — Phys.Lett., 1993, v.B304; MSUHEP 93-18.
7. **Sjostrand T.** — Comput.Phys.Commun., 1986, v.39, p.38;
   Sjostrand T., Begtsson M. — Comput.Phys.Commun., 1987, v.53, p.367;
   Sjostrand T. — CERN-TH.7112/93.
8. **Gluck M., Hoffmann E., Reya E.** — Z.Phys., 1982, v.C13, p.119.
9. **Higgs P.** — Phys.Lett., 1964, v.12, p.132;
   Englert F., Brout R. — Phys.Rev.Lett., 1964, v.13, p.321.
10. See for example: **Ta-Pei Cheng, Ling-Fong-Li** — Gauge Theory of Elementary Particle Physics (Oxford University Press, Oxford, 1984);
    Pokorsky S. — Gauge Field Theories (Cambridge University Press, Cambridge, 1987);
    Borodulin V.I., Rogalyov R.N., Slabospitsky S.R. — IHEP Preprint 95-50.
11. Review of Particle Properties, — Phys.Rev., 1994, v.D50, p.1173.
12. **Blondel A.** — Precision Electroweak Physics at LEP, CERN-PPE/94-133 (1994).
13. **Lee B.W., Quigg C., Thacker C.D.** — Phys.Rev.Lett., 1977, v.38, p.883; Phys.Rev., 1974, v.D10, p.1145.
14. **Cabibbo N., Maiani L., Parisi G., Petronzio R.** — Nucl.Phys., 1979, v.B158, p.295;
    Lindner M. — Z.Phys., 1986, v.C31, p.295.

15. **Krasnikov N.V.** — Yad.Fiz., 1978, v.28, p.549;
Hung P.Q. — Phys.Rev.Lett., 1979, v.42, p.873;
Politzer H.D., Wolfram S. — Phys.Lett., 1979, v.B82, p.242; **Anselm A.A.** — JETP Lett., 1979, v.29, p.590; **Lindner M., Sher M., Zaglauer M.** — Phys.Lett., 1989, v.B228, p.139.
16. **Krasnikov N.V., Kreyerhoff G., Rodenberg R.** — Mod.Phys.Lett., 1994, v.A9, p.3663.
17. **Georgi H. et al.** — Phys.Rev.Lett., 1978, v.40, p.692.
18. See for example: **Gunion J.F., Haber H.E., Kane G., Dawson S.** — The Higgs Hunter's Guide (Addison-Wesley Publishing Company, Redwood City, CA) 1990.
19. See for example: **Altarelli G., Kleiss R., Verzegnassi C.,** editors. — Physics at LEP, vol. 1: Standard Physics, CERN Yellow Report 86-02 (1986).
20. **Peccei R.D., Quinn H.R.** — Phys.Rev.Lett., 1977, v.38, p.1440; **Baluni V.** — Phys.Rev., 1979, v.D19, p.2227;
Crewther R.J. et al. — Phys.Lett., 1979, v.B88, p.123; 1990, v.91, p.487.
21. See for example: **Bigi I.I. et al.** — In: CP-Violation, edt.C.Jarlskog (World Scientific, Singapore, 1989);
Buras A.J. — Nucl.Instr. and Meth. in Phys.Res., 1995, v.A308, p.1;
Gronau M. — Nucl.Instr. and Meth. in Phys.Res., 1995, v.A368, p.21;
Neubert M. — Mod.Phys., 1996, v.A11, p.4173.
22. **Wolfenstein L.** — Phys.Rev.Lett., 1983, v.51, p.1945.
23. See for examle: **Neubert N.** — Mod.Phys., 1996, v.A11, p.4173.
24. **Chau L.L., Keung W.Y.** — Phys.Rev.Lett., 1984, v.53, p.1802;
Jarlskog C., Stora R. — Phys.Lett., 1988, v.B208, p.268.
25. **Shifman M.A., Vainstein A.I., Zakharov V.I.** — Nucl.Phys., 1977, v.B120, p.316.
26. **Krisebom K. et al.** — (LHC-B), Letter of intent, CERN/LHCC 95-5, 1995.
27. **Nakada T.** — In: Proceedings of the 3rd German-Russian Workshop on Heavy Quark Physics. Editors: M.A.Ivanov and V.E.Lybovitskij, Dubna, 1996.
28. **Ali A.** — CKM Update: a Review, Workshop Beauty-94, Mt.St.Michel, France, May, 1994, Nucl.Instrum.Methods, 1994, v.A351, p.95.
29. **Denegri D. et al.** — Nucl.Instrum.Methods, 1994, v.A351, p.95.
30. **Ali A., Creub C., Mannel T.** — Rare B-Decays in Standard Model, DESY 93-016 (1993).
31. See for instance: **Eggers H.C., Rafelski J.** — Mod.Phys., 1991, v.A6, p.1067;
Singh C.P. — Mod.Phys., 1992, v.A7, p.7185;
Jacob M. — Mod.Phys., 1996, v.A11, p.4943.
32. **Matsui T., Satz H.** — Phys.Lett., 1986, v.B178, p.416.
33. NA50, LAPP/Annecy-Bucharest IAP-Cagliari U. — CERN-LPC/Clermont-Ferrand-Cracow IPN, LIP/Lisbon-Moscow INR-Orsay
IPN-Orsay, LPNHE-Ecole Poly./Palaiseau-Strasbourg CNR et U. — Torino U. — Lyon IPN Collaboration.
34. **Gershell G., Hufner J.** — Phys.Lett., 1988, v.B207, p.257;
Ftanik J., Lichard P., Pisut J. — Phys.Lett., 1988, v.B207, p.194;
Gavin S., Gyulassy M., Jackson A. — Phys.Lett., 1988, v.B207, p.257.
35. ALICE, Technical Proposal, CERN/LHCC/95-71(1995).
36. **Kvatadze R., Shanidze R.** — CERN CMS TN/94-270 (1994).
37. Reviews and original references can be found in: **Barbieri R.** — Riv.Nuovo Cim.,1988,v.11,p.1;
Lahanus A.B., Nanopoulos D.V. — Phys.Rep., 1987, v.145, p.1;
Haber H.E., Lane G.L. — Phys.Rep., 1985, v.117, p.75;
Nilles H.P. — Phys.Rep., 1984, v.110, p.1.
38. **Ferrara S., Freedman D.Z., Van Nieuwenhuizen P.** — Phys.Rev., 1976, v.D13, p.3214;
Deser S., Zumino B. — Phys.Lett., 1976, v.B62, p.335;
Van Nieuwenhuizen P. — Phys.Rep., 1981, v.68, p.189;
Wess J., Bagger J. — Supersymmetry and Supergravity (Princeton University Press, Princeton, NJ, 1983).

39. See for example: **Green M.B., Schwarz J.H., Witten E.** — Superstring Theory, Cambridge Press, 1987.
40. See for example: **Dreiner H., Ross G.G.** — Nucl.Phys., 1991, v.B365, p.597.
41. **Polonsky N., Pomarol A.** — Phys.Rev.Lett., 1994, v.73, p.2292.
42. **Krasnikov N.V., Popov V.V.** — INR Preprint 976TH/96.
43. **Ibanez L.E., Lopez C.** — Phys.Lett., 1983, v.126B, p.54; Nucl.Phys., 1984, v.B233, p.511; Nucl.Phys., 1985, v.B256, p.218.
44. See references 37.
45. **De Boer W., Ehret R., Kazakov D.I.** — Z.Phys., 1995, v.C67, p.647.
46. **Ellis J., Ridolfi G., Zwirner F.** — Phys.Lett., 1991, v.B257, p.83;
Haber H., Hempfling R. — Phys.Rev.Lett., 1991, v.66, p.1815;
Yamada A. — Phys.Lett., 1991, v.B263, p.233;
Barbieri R., Frigeni M., Caravaglis F. — Phys.Lett., 1991, v.B258, p.233;
Chanowski P.M., Pokorski S., Rosick J. — Phys.Lett., 1992, v.B275, p.191.
47. **Krasnikov N.V., Pokorski S.** — Phys.Lett., 1992, v.B288, p.184.
48. **Baer H. et al.** — Low Energy Supersymmetry Phenomenology, CERN-PPE/95-45.
49. **Baer H. et al.** — Phys.Lett., 1985, v.B161, p.175;
Gamberini G. — Z.Phys., 1986, v.C30, p.605;
Baer H. et al. — Phys.Rev., 1987, v.D36, p.96;
Gamberini G. et al. — Phys.Lett., 1988, v.B203, p.453;
Barnett R.M., Gunion J., Haber H. — Phys.Rev., 1988, v.D37, p.1892;
Bartl A. et al. — Z.Phys., 1991, v.C52, p.477.
50. See for example: **Baer H. et al.** — Mod.Phys., 1989, v.A4, p.4111.
51. **Kunszt Z., Zwirner F.** — Nucl.Phys., 1992, v.B385, p.3.
52. **Abddullin S.** — In: SUSY Studies in CMS, LHCC/SUSY Workshop, CERN, October 29-30, 1996.
53. **Iashvili I.** — In: SUSY Studies in CMS, LHCC/SUSY Workshop, CERN, October 29-30, 1996.
54. **Denegri D., Rurua L., Stepanov N.** — CERN CMS TN/96-059, October 1996.
55. **Krasnikov N.V.** — Mod.Phys.Lett., 1994, v.A9, p.791;
Krasnikov N.V. — Phys.Lett., 1996, v.B388, p.783;
Arkani-Hamed N. et al. — Phys.Rev.Lett., 1996, v.77, p.1937.
56. **Krasnikov N.V.** — Zhetp.Lett., 1977, v.65, p.139.
57. **Dimopoulos S. et al.** — Phys.Rev., 1990, v.D41, p.2099;
Dawson S. — Nucl.Phys, 1985, v.B261, p.297;
Binetruy P., Gunion J. — INFN Eloisatron Project Working Group, 6th Workshop on Novel Features of High-Energy Hadronic Collision, Erice, 1988;
Dreiner H., Ross G.G. — Nucl.Phys., v.B365, p.597.
58. **Krasnikov N.V.** — Phys.Lett., 1996, v.B386, p.161.
59. **Krasnikov N.V.** — Phys.Lett., 1993, v.B306, p.283;
Krasnikov N.V., Kreyerhoff G., Rodenberg R. — Nuovo Cimento, 1994, v.A107, p.589.
60. **Krasnikov N.V.** — Preprint ENSLAPP-A-529-95; JETP. Lett., 1995, v.61, p.236.
61. **Antoniadis I., Benakli K., Quiros M.** — Phys.Lett., 1994, v.B331, p.313.
62. **Banks T., Dixon L.** — Nucl.Phys., 1988, v.B307, p.93;
Antoniadis I., Bachas C., Lewellen D., Tomaros T. — Phys.Lett., 1988, v.B207, p.441.
63. **Antoniadis I.** — Phys.Lett., 1990, v.B246, p.377.
64. **Antoniadis I., Munoz C., Quiros M.** — Nucl.Phys., 1993, v.B397, p.515.
65. **Antoniadis I., Benakli K.** — Preprint CPTH-A 0793(1993).
66. **Krasnikov N.V.** — Mod.Phys.Lett., 1995, v.A10, p.2675.
67. See for example: **del Agulia F.,Ametller Ll.,Kane G.L., Vidal J.** — Nucl.Phys.,1990,v.B334,p.1.